On the relationship between sub-daily instantaneous and daily total gross primary production: Implications for interpreting satellite-based SIF retrievals

Yao Zhang[a,*], Xiangming Xiao[a,b,*], Yongguang Zhang[c], Sebastian Wolf[d], Sha Zhou[e], Joanna Joiner[f], Luis Guanter[g], Manish Verma[h], Ying Sun[i], Xi Yang[j], Eugénie Paul-Limoges[d,k], Christopher M. Gough[l], Georg Wohlfahrt[m], Beniamino Gioli[n], Christiaan van der Tol[o], Nouvellon Yann[p], Magnus Lund[q], Agnès de Grandcourt[p,r]

[a] *Department of Microbiology and Plant Biology, Center for Spatial Analysis, University of Oklahoma, Norman, OK 73019, USA*
[b] *Ministry of Education Key Laboratory of Biodiversity Science and Ecological Engineering, Institute of Biodiversity Science, Fudan University, Shanghai 200433, China*
[c] *Jiangsu Provincial Key Laboratory of Geographic Information Science and Technology, International Institute for Earth System Sciences, Nanjing University, 210023 Nanjing, China*
[d] *Department of Environmental Systems Science, ETH Zurich, 8092 Zurich, Switzerland*
[e] *State Key Laboratory of Hydroscience and Engineering, Department of Hydraulic Engineering, Tsinghua University, Beijing, China*
[f] *NASA Goddard Space Flight Center, Greenbelt, MD, USA*
[g] *Helmholtz Center Potsdam, GFZ German Research Center for Geosciences, Remote Sensing Section, Telegrafenberg A17, 14473 Potsdam, Germany*
[h] *Consulting for Statistics, Computing & Analytics Research, University of Michigan, Ann Arbor, MI 48109, USA*
[i] *School of Integrative Plant Science, Cornell University, Ithaca, NY 14853, USA*
[j] *Department of Environmental Sciences, University of Virginia, Charlottesville, VA 22903, USA*
[k] *Remote Sensing of Water Systems, University of Zurich, Switzerland*
[l] *Virginia Commonwealth University, Department of Biology, Richmond, VA 23284-2012, USA*
[m] *University of Innsbruck, Institute of Ecology, Sternwartestraße 15, A-6020 Innsbruck, Austria*
[n] *Consiglio Nazionale delle Ricerche, Instituto di Biometeorologia, via Giovanni Caproni 8, I-50145 Firenze, Italy*
[o] *Department of Water Resources, Faculty ITC, University of Twente, 7500 Enschede, The Netherlands*
[p] *CIRAD, UMR Eco&Sols, 2 place Viala, 34060 Montpellier, France*
[q] *Department of Bioscience, Arctic Research Centre, Aarhus University, Frederiksborgvej 399, DK-4000 Roskilde, Denmark*
[r] *Centre de Recherche sur la Durabilité et la Productivité des Plantations Industrielles, BP 1291 Pointe-Noire, Congo*

ARTICLE INFO

ABSTRACT

Spatially and temporally continuous estimation of plant photosynthetic carbon fixation (or gross primary production, GPP) is crucial to our understanding of the global carbon cycle and the impact of climate change. Besides spatial, seasonal and interannual variations, GPP also exhibits strong diurnal variations. Satellite retrieved solar-induced chlorophyll fluorescence (SIF) provides a spatially continuous, but temporally discrete measurement of plant photosynthesis, and has the potential to be used to estimate GPP at global scale. However, it remains unclear whether the seasonal time series of SIF snapshots taken at a fixed time of the day can be used to infer daily total GPP variation at spatial and seasonal scales. In this study, we first used GPP estimates from 135 eddy covariance flux sites, covering a wide range of geographic locations and biome types, to investigate the relationship between the instantaneous GPP (GPP_{inst}) and daily GPP (GPP_{daily}) on the seasonal course for different times of the day. Latitudinal and diurnal patterns were found to correspond to variations in photosynthetically active radiation (PAR) and light use efficiency (LUE), respectively. We then used the Soil-Canopy Observation Photosynthesis and Energy Balance (SCOPE) model and the FluxCom GPP product to investigate the instantaneous and daily SIF-GPP relationships at five flux tower sites along a latitudinal gradient and at a global scale for different biome types. The results showed that daily SIF had a stronger linear correlation with daily GPP than instantaneous SIF at the seasonal scale, with an instantaneous to daily SIF conversion factor following the latitudinal and seasonal pattern driven by PAR. Our study highlights the necessity to take the latitudinal and

diurnal factors into consideration for SIF-GPP relationship analyses or for physiological phenology analyses based on SIF.

1. Introduction

Photosynthetic carbon fixation by plants is the most influential CO_2 flux connecting the atmosphere and the biosphere. Every year, approximately 120 Pg carbon is fixed by the terrestrial ecosystems through photosynthesis, providing food and materials for human beings while also largely driving the global carbon cycle (Beer et al., 2010). The underlying ecophysiological mechanisms controlling this biochemical process have been long studied, mostly at leaf or molecular scale (Farquhar et al., 1980; Krause and Weis, 1991). Actual estimation of the photosynthetic exchange flux at the ecosystem scale, also known as gross primary productivity (GPP), only became practical in the 1990s with the emergence of the eddy covariance (EC) technique (Baldocchi et al., 2001). EC flux towers measure the net ecosystems exchange (NEE) which can be further partitioned into GPP and ecosystem respiration (Lasslop et al., 2010; Reichstein et al., 2005; Wohlfahrt and Gu, 2015). These ground observations have been critical to the development and testing of models used to simulate GPP at a larger scale, but the performance of these models is still not satisfactory, with large discrepancies existing among different models (Anav et al., 2015). Using observations as a constraint can help to improve the model performance so that models may better predict the global carbon cycle under future climate scenarios (Luo et al., 2011; Peng et al., 2011). However, the sensitivity of different sub-modules, parameters or input variables are usually associated with GPP variations at different time or spatial scales, which need to be taken into consideration when conducting this model-data fusion.

Plant photosynthesis is powered by light and affected by numerous environmental factors and plant phenology. Its variation is often characterized by four aspects:

(1) Diurnal variation: as the solar radiation has a diurnal cycle, it directly affects the incoming energy and carbon assimilation of plants. Other environmental or physiological variables affecting stomatal conductance and CO_2 uptake, such as air temperature, vapor pressure deficit (VPD), or leaf water potential also show diurnal cycles.
(2) Seasonal variation: driven by the climate (e.g., temperature, water availability, radiation) seasonality and plant phenology, it represents one of the most important components of GPP overall variability. Most in situ and remote observations are also conducted at this scale.
(3) Spatial variation: due to the spatial distribution of plant species, latitudinal pattern of incoming solar radiation, topography, and spatial variations in climate and soil properties, GPP also exhibits strong spatial variations.
(4) Interannual variation: usually driven by climate anomalies and land cover changes, it is one order of magnitude smaller than other types of variations and is therefore the most challenging level for models to simulate accurately (Verma et al., 2015).

For some methods, e.g., the eddy covariance (EC) technique, a single site can capture ecosystem to landscape-scale diurnal, seasonal, and interannual variations because continuous measurements occur at a high sampling frequency (Aubinet et al., 2012). However, EC sites are spatially dispersed and, therefore, cannot provide spatially continuous measurements (Schimel et al., 2015). In contrast, remote sensing technologies usually have high spatial coverage with polar orbiting (low Earth orbiting, LEO) satellites, while the continuous temporal sampling is generally not possible. For LEO satellite platforms, we can only get from zero to possibly a few observations per day depending on the swath width of the instrument and latitude (multiple observations per day with a single instrument are only possible at high latitudes and with a wide swath instrument, e.g. (Guanter et al., 2015)). If observing conditions are not favorable, e.g., owing to clouds or aerosols, a valid observation may not be present over several days (Sims et al., 2005). For optical remote sensing that uses vegetation indices (VIs) to quantify vegetation canopy and leaf properties that change relatively slowly, usually over the course of weeks to months, this low sampling frequency is adequate to quantify the spatial, seasonal and interannual variations (Guan et al., 2015; Huete et al., 2006; Zhang et al., 2016b). The diurnal variation of satellite observed VI (an indicator of vegetation greenness) or canopy coverage is mostly caused by leaf inclination or bidirectional reflectance (Los et al., 2005). As long as the satellite overpass time is stable, these effects are minor and a VI measurement at most time of the day (when the satellite and solar zenith angles are low) may be a good proxy of the VI for that day (Chen, 1996). However, as the sun-sensor geometry also gradually changes at seasonal scales, seasonal dynamics of VIs should take this effect into consideration, especially in tropical regions where backscattering and forward scattering shift within a year (Bi et al., 2015; Morton et al., 2014).

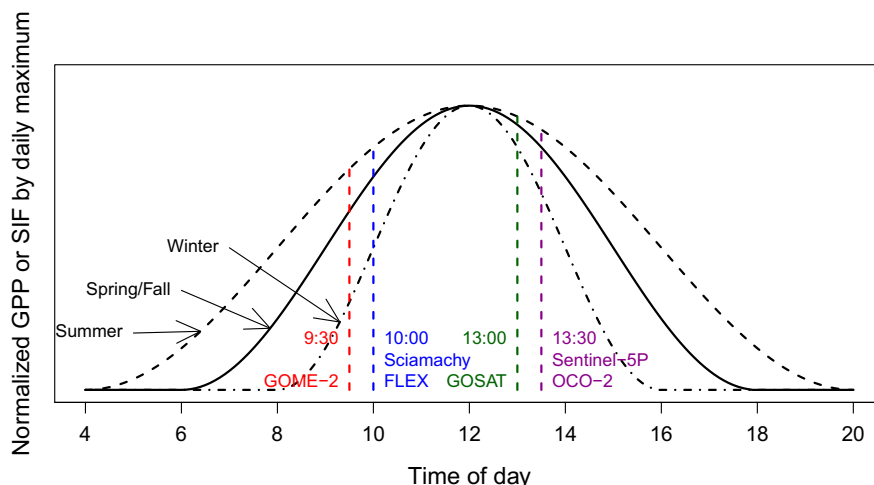Following the successful retrieval of solar-induced chlorophyll

Fig. 1. Schematic graph showing the diurnal course of GPP or SIF normalized by their daily maximum values. These schematic curves are shown for different seasons. Overpass time (solar time) of different satellites/sensors measuring SIF are also indicated.

fluorescence (SIF) signals from satellite sensors (Frankenberg et al., 2011; Joiner et al., 2013, 2012), we have access to a new type of spatially extensive vegetation observation, which is based on energy re-emitted by plants rather than reflected. SIF is a small amount of energy re-emitted during the light reaction of the photosynthesis process (Baker, 2008; Porcar-Castell et al., 2014). Studies have shown that it is

highly correlated with the energy absorbed by chlorophyll pigments and the photosynthetic electron transport (Zhang et al., 2014, 2016d). Like GPP, SIF is also driven by photosynthetically active radiation (PAR), and has a strong diurnal cycle embedded within the seasonal, spatial, and interannual variations. Previous studies attempted to use satellite-based SIF to estimate GPP, however, this relationship was only
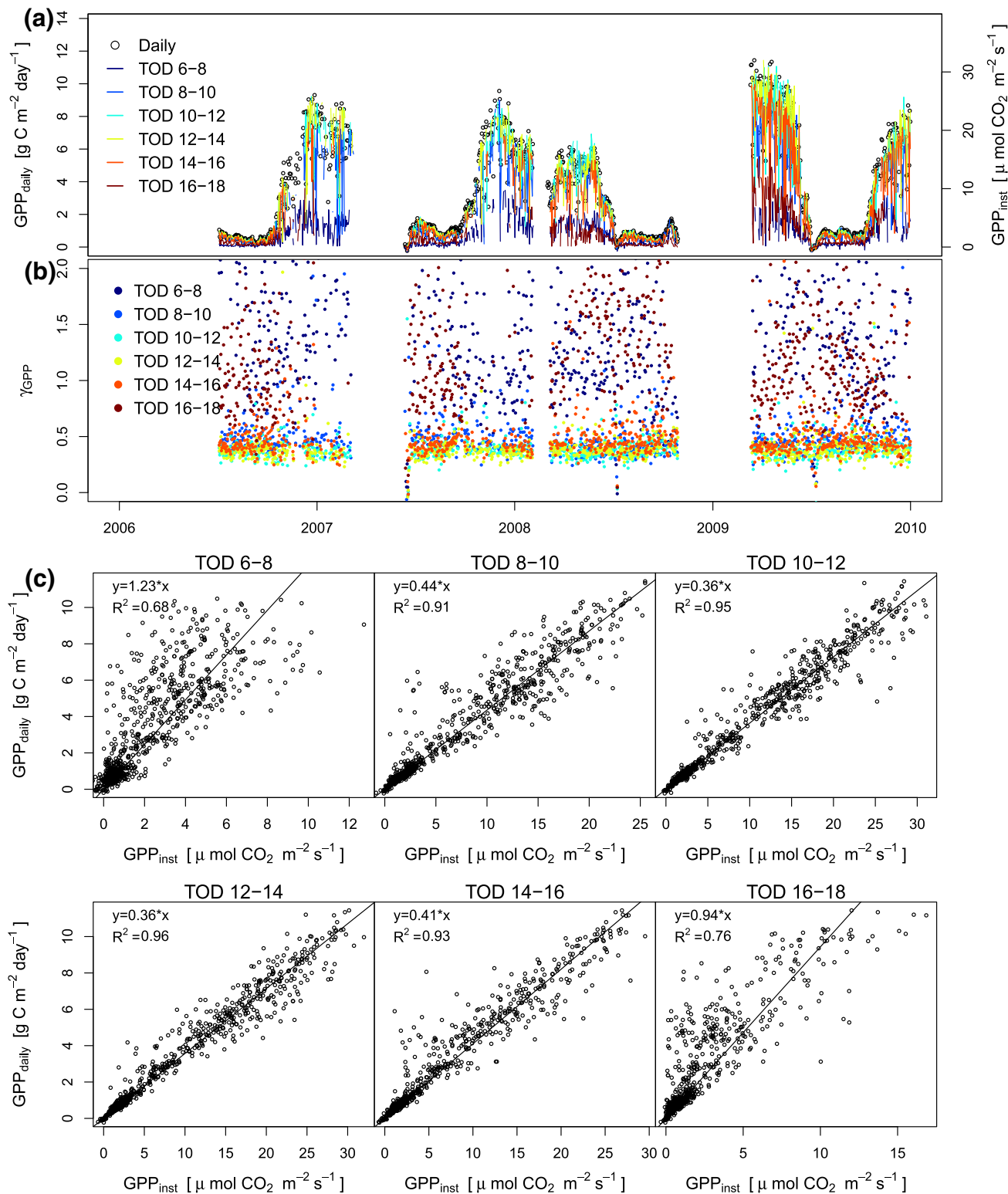

Fig. 2. Seasonal variation of (a) GPP_{inst}, GPP_{daily}, and (b) γ_{GPP} of different time of day from a savanna flux tower site CG-Tch. (c) The regression between GPP_{daily} and GPP_{inst} from different times of the day (TOD). R^2 and the regression slope for each TOD are shown at the top left corner and will be used for cross-site statistics. Large gaps in 2007 and 2009 are observations that did not pass the quality checks. Note that the units for GPP_{daily} (g C m^{-2} day^{-1}) and GPP_{inst} (µmol CO_2 m^{-2} s^{-1}) are different.

tested at individual sites for cropland or broadleaf forest (Guanter et al., 2014; Wagle et al., 2016; Yang et al., 2015). Moreover, these studies mostly compared satellite derived instantaneous SIF with the daily GPP. The discrepancies between the underlying different temporal scales, i.e., instantaneous SIF observation at satellite overpass time vs. daily integrated GPP, so far have not been fully evaluated.

Previous studies have shown that SIF and GPP are linked through the photon partitioning after absorption by plant chlorophyll (Genty et al., 1989). Absorbed photons undergo three different pathways (i) entering the electron transport chain (ETC) and generate chemical energy further used for the Calvin Cycle (ϕ_P), (ii) being dissipated as heat (ϕ_D), or (iii) being reemitted as fluorescence (ϕ_F). The symbol ϕ represents the quantum yield for each pathway. These mechanisms can be used to build up the link between instantaneous GPP and SIF (Damm et al., 2010; van der Tol et al., 2014, 2009a). Many studies have investigated these relationships at the scale of sub-seconds to minutes, but the spatial and seasonal variation of this relationship remains unclear (Porcar-Castell et al., 2014). In addition, because SIF measurements from satellites are usually not continuous over time, we still need to understand the scale conversion from instantaneous to daily sums, i.e., whether a snapshot of photosynthetic activity at a specific time of the day can represent the daily total carbon fixation at both spatial and temporal (seasonal and interannual) scales. Sims et al. (2005) and Ryu et al. (2012) showed that the midday value of GPP or ET can be a representative of daily or 8-day value. But those studies only focused on a limited number of sites and the MODIS overpass time (10:00–11:00 and 13:00–14:00). As the satellites from which SIF retrievals can be made have different overpass times (Fig. 1), it is unclear how that can affect the relationships between instantaneous SIF and daily GPP at different locations.

This study aims to fill those gaps with both observations and modeling approach: we used eddy flux data from 135 sites, covering a wide range of geographical regions and biome types, the global GPP product from FluxCom, and SIF from Global Ozone Monitoring Experiment 2 (GOME-2) and Orbiting Carbon Observatory 2 (OCO-2), to explore the instantaneous-daily relationship among GPP, PAR, light use efficiency (LUE) and SIF. In particular, we focused on the following questions which have not yet been addressed: (1) What is the relationship between the daily total GPP and instantaneous GPP at different times of day (TOD) and different locations? (2) What is the cause of these spatial and temporal patterns? (3) Does SIF also exhibit these spatio-temporal patterns and how does this affect our interpretation of the SIF-GPP relationship? Besides these three main objectives, we also discussed how the instantaneous and daily SIF-GPP relationships affect the retrieval of phenology using satellite based SIF data.

2. Materials and method

2.1. GPP from FLUXNET data base and preprocessing

We used eddy flux data (Baldocchi et al., 2001) from 135 sites covering a large variety of biome types. The flux dataset was acquired from the FLUXNET 2015 release (December 2015, http://fluxnet.fluxdata.org/data/fluxnet2015-dataset/) (Pastorello et al., 2017). The spatial distribution and the information about each site can be found in Supporting Information (Fig. S1, Table S1). This dataset was processed using a standardized protocol, which enabled us to make a cross-site comparison (http://fluxnet.fluxdata.org/data/fluxnet2015-dataset/data-processing/) (Barr et al., 2013; Papale et al., 2006; Vuichard and Papale, 2015). To answer the question whether the seasonal cycle of instantaneous GPP (GPP$_{inst}$) at a certain time of day can represent the seasonal cycle of the daily GPP (GPP$_{daily}$), we used both the original half-hourly data and the daily data. The half-hourly data were aggregated into 2-hour bins from 6:00 am to 6:00 pm to represent the GPP$_{inst}$. A rigorous data quality check was applied during this aggregation process: 1) Only the half-hourly and daily data in the weeks

with more than 75% of valid (not gap-filled) radiation and net ecosystem exchange (NEE) observations were used. 2) To reduce the uncertainty related to the NEE partitioning, we compared the daily total GPP estimates from both the daytime method (light response curve; Lasslop et al., 2010) and the nighttime method (nighttime NEE as respiration; Reichstein et al., 2005). The GPP estimation was considered unbiased only if the difference of GPP from both methods were within 20% of their average or within $2 \, g \, C \, m^{-2} \, day^{-1}$, in which case GPP was then calculated as the average of both methods. We found that this criterion performed well and most rejected data were extrapolated for very long gaps with low reliability. In addition, we also analyzed the instantaneous and daily GPP relationships using GPP estimated from either the daytime method or the nighttime method, as a support for the robustness of our findings. We did not use the original half-hourly data as it would generate too many GPP$_{inst}$-GPP$_{daily}$ comparisons; six two-hour bins were enough to get the diurnal change of their relationship.

2.2. Relationship between instantaneous and daily GPP at seasonal scale across sites

The relationship between daily GPP (GPP$_{daily}$) and instantaneous GPP (GPP$_{inst}$) can be built for each day using a conversion factor (γ_{GPP}):

$$\gamma_{GPP} = \frac{GPP_{daily}}{GPP_{inst}} \tag{1}$$

The GPP$_{daily}$ (in $g \, C \, m^{-2} \, day^{-1}$) was calculated as the cumulative summation of half hour GPP (expressed in $\mu mol \, CO_2 \, m^{-2} \, s^{-1}$ in the FLUXNET2015 dataset), but was converted to $\mu mol \, CO_2 \, m^{-2} \, s^{-1}$ (representing the average instantaneous GPP over a 24-hour period) when compared with GPP$_{inst}$. γ_{GPP} can be calculated for each site each day at seasonal scale. If γ_{GPP} at one site has little variation across time, it indicates that GPP$_{inst}$ can represent GPP$_{daily}$ at temporal scale. Similarly, if γ_{GPP} has little variation across sites, it indicates that GPP$_{inst}$ can represent GPP$_{daily}$ at across sites. For simplicity, we built linear regressions with zero intercept between GPP$_{daily}$ and GPP$_{inst}$ for each site at seasonal scale; a high R^2 indicates γ_{GPP} is seasonally stable for a given site and γ_{GPP} can be calculated as the regression slope (Fig. 2). The variability of regression slopes (γ_{GPP}) across sites is indicative of the variability of the relationship across space.

2.3. Relationship between instantaneous and daily LUE at seasonal scale across sites

LUE is a very important parameter that connects light absorption by the ecosystem and the carbon fixation through photosynthesis (Monteith, 1972). The instantaneous and daily light use efficiency (LUE$_{inst}$ and LUE$_{daily}$, respectively) are defined as follows:

$$LUE_{inst} = \frac{GPP_{inst}}{fPAR \times PAR_{inst}} \tag{2}$$

$$LUE_{daily} = \frac{GPP_{daily}}{fPAR \times PAR_{daily}} \tag{3}$$

The GPP$_{inst}$ and PAR$_{inst}$ were also averaged over 2 h from 6:00 am to 6:00 pm local time for each site. For simplicity, both daily GPP and PAR are in the same unit as instantaneous GPP and PAR, representing the average value of a 24-hour period. Within one day, the diurnal variation of the fraction of the PAR absorbed by the canopy (fPAR) is relatively small (Fensholt et al., 2004) and is neglected. Following the definition of γ_{GPP}, we can also define the γ_{LUE}, i.e., the ratio of LUE$_{daily}$ over LUE$_{inst}$.

$$\gamma_{LUE} = \frac{LUE_{daily}}{LUE_{inst}} = \frac{\frac{GPP_{daily}}{APAR_{daily}}}{\frac{GPP_{inst}}{APAR_{inst}}} \approx \frac{\frac{GPP_{daily}}{PAR_{daily}}}{\frac{GPP_{inst}}{PAR_{inst}}} = \frac{ELUE_{daily}}{ELUE_{inst}} \tag{4}$$

where the ELUE represents the ecosystem LUE and is calculated as $\frac{GPP}{PAR}$.

Similarly, we did not calculate γ_{LUE} for each day, but used the regression slope between daily and instantaneous ecosystem LUE ($ELUE_{daily} = \frac{GPP_{daily}}{PAR_{daily}}$ and $ELUE_{inst} = \frac{GPP_{inst}}{PAR_{inst}}$, respectively) for each site. The use of ELUE rather than LUE avoided the uncertainties related to the calculation of fPAR.

2.4. Analytical conversion from instantaneous to daily APAR

Both SIF and GPP are driven by the incident solar irradiance and therefore both exhibit a diurnal cycle. Thus, the relationship between the daily APAR ($APAR_{daily}$) and instantaneous APAR ($APAR_{inst}$) is very important to determine the relationship between SIF_{daily} and SIF_{inst}, and GPP_{daily} and GPP_{inst}. As diurnal changes in incoming solar radiation are mostly determined by the solar zenith angle (SZA), we can calculate the conversion factor between $APAR_{inst}$ and $APAR_{daily}$ (γ_{APAR}) as below:

$$\gamma_{APAR} = \frac{APAR_{daily}}{APAR_{inst}} \approx \frac{PAR_{daily}}{PAR_{inst}} \approx \frac{\cos(SZA)_{daily}}{\cos(SZA)_{inst}} \tag{5}$$

This approach did not consider the minor diurnal variation of fPAR and the cloud and atmospheric scattering effect on PAR. The cos $(SZA)_{daily}$ can be calculated following the method documented in Frankenberg (2015):

$$\cos(SZA)_{daily} = \int_{t+12h}^{t-12h} \cos(SZA(t))dt \tag{6}$$

The SZA for each site was calculated using the "RAtmosphere" package (https://cran.r-project.org/web/packages/RAtmosphere/index.html) in R language (https://www.r-project.org/). The "SZA" function can calculate the SZA of a specific location based on its latitude, date, and local time of day. The instantaneous SZA was calculated at a local time between 7:00 to 17:00 with a time-step of 2 h corresponding to the mid-time of each GPP aggregation bin. The cos $(SZA)_{daily}$ was calculated numerically as the integral of cos(SZA(t))dt at a 10-minute time-step. Similarly, we used a linear regression between cos$(SZA)_{daily}$ and cos$(SZA)_{inst}$ to estimate γ_{APAR} at different times of the day (TOD). The regression was forced to pass through the origin and the regression slope represented γ_{APAR} for a specific location. Because SZA is a function of local time and latitude, γ_{APAR} only varies with time and latitude.

2.5. SCOPE model simulations

To investigate the relationship between instantaneous and daily SIF (SIF_{inst} and SIF_{daily}, respectively), and the GPP and SIF relationship both at bi-hourly and daily scales, we used the SCOPE model (van der Tol et al., 2014, 2009b) to simulate both SIF and GPP. SIF_{daily} was calculated as the average of all half-hourly SIF_{inst} within each 24-hour period. To test whether γ_{SIF} (SIF_{daily}/SIF_{inst}, unitless) also exhibits a latitudinal pattern similar to GPP, we selected five grassland or savannas sites (DK-ZaH, US-Ivo, DK-Eng, US-Var, CG-Tch) along the latitude where the cosines of latitudes of these sites are close to 0.2, 0.4, 0.6, 0.8, and 1 (Table S1, Fig. S1). We chose the grassland/savannas biome types since they are broadly distributed at different latitudes and their canopy structure is relatively simple. Except CG-Tch, all other sites are dominated by C3 species, C3 and C4 pathways were simulated differently in the SCOPE model. US-Var and CG-Tch also have sparse tree coverage in the GOME-2 SIF and EVI/MTCI footprint ($0.5° \times 0.5°$ and 5 km × 5 km, respectively), while the tree coverage in the flux tower footprint is relatively low. This can cause inconsistency when validating model simulation with flux tower measurements and satellite observations.

Chlorophyll $a + b$ content (Cab), maximum carboxylation rate (V_{cmax}) and the leaf area index (LAI) are the most influential parameters for simulating SIF and GPP with the SCOPE model (Verrelst et al., 2015; Zhang et al., 2016a). For Cab, we followed the method used in previous studies (Zhang et al., 2014; Zhang et al., 2016a). The Cab was inversely

estimated from a lookup table generated by the forward simulation of the PROSPECT model with a large number of parameter combinations. The 8-day Enhanced Vegetation Index (EVI) and MERIS Terrestrial Chlorophyll Index (MTCI Dash and Curran, 2004) for those five sites were used as inputs and Cab was inverted at 8-day intervals. All other climate inputs were obtained from the flux tower measurements, and the LAI was obtained from the MODIS LAI product using the Oak Ridge National Laboratory MODIS global subsets tool with a footprint of 5 km to match with that of MTCI (https://modis.ornl.gov/cgi-bin/MODIS/GLBVIZ_1_Glb/modis_subset_order_global_col5.pl). The maximum carboxylation rate at 25 °C (V_{cmax}) were set to constant for each site following previous studies (52 $\mu mol\ m^{-2}\ s^{-1}$ for C3 grass and 30 $\mu mol\ m^{-2}\ s^{-1}$ for C4 grass) (Kattge et al., 2009; Wullschleger, 1993; Zhang et al., 2016a). The canopy height was set to 0.5 m throughout the growing season and the leaf inclination angle distribution was empirically set to spherical (Asrar et al., 1986). These parameter settings may introduce uncertainties, but are thought to have limited effects on the instantaneous-daily relationship (Verrelst et al., 2015, 2016). Other unspecified parameters were set to their default values for each ecosystem type in SCOPE v1.61 (https://github.com/Christiaanvandertol/SCOPE).

2.6. Comparison of satellite retrieved SIF and GPP at global scale

Since SIF can also be expressed as a function of APAR (SIF = APAR × FE, FE: apparent fluorescence efficiency), we can approximate SIF_{daily} from SIF_{inst} by assuming that FE has little variation at a diurnal scale. This is a first-order approximation since two contributing factors of FE, namely quantum yield for fluorescence (ϕ_F) and escape coefficient for near-infrared SIF (f_{esc}, how much SIF emitted by individual leaf can escape the canopy without being re-absorbed by other leaves) have a much smaller variation compared to the diurnal variation of PAR (data not shown), especially at the far-red band. The SIF_{daily} can be approximated as:

$$SIF_{daily} \approx \frac{APAR_{daily}}{APAR_{inst}}SIF_{inst} \approx \frac{PAR_{daily}}{PAR_{inst}}SIF_{inst} \tag{7}$$

where SIF_{inst} is the satellite retrieved SIF and PAR_{daily} is analytically estimated from SZA, PAR_{inst} can be estimated from the SZA when the observation was made, which is embedded in the GOME-2 and OCO-2 SIF product. We did not use the PAR_{inst} for the satellite overpass time (e.g., 9:30 am for GOME-2 and 1:30 pm for OCO-2) since that overpass time only applies for equator, higher latitudes may have some variation. In this study, we used both the GOME-2 SIF v26 product from the MetOp-A satellite (Joiner et al., 2013, 2016), and the OCO-2 SIF Lite product (B7101r) (Frankenberg, 2015; Frankenberg et al., 2014). The MetOp-A satellite has an overpass time of ~9:30 am and SIF was retrieved around the wavelength of 740 nm using a principle component analysis algorithm (Joiner et al., 2013). These retrievals had a footprint of 40 km × 80 km (40 km × 40 km after 15 July 2013) and were further aggregated to a 0.5° × 0.5° monthly gridded product. The OCO-2 SIF was retrieved around 757 nm using an iterative least squares fitting technique. Each day, around 100,000 soundings were collected on land with a footprint of ~2 km × 1.3 km. We aggregated the raw SIF retrievals to monthly 0.5° × 0.5° gridded product following the quality check instructions. Since this dataset only became available since September 2014, it cannot be directly compared with GPP dataset. We used 2 year of data (2015, 2016) to calculate the average SIF of each month. In this way, we ignored the interannual variation and focused on the seasonal variation.

We used the monthly GPP product from FluxCom with a spatial resolution of 0.5° × 0.5°. The FluxCom GPP was generated using three machine learning algorithms, combined with GPP estimated from the daytime method (Lasslop et al., 2010) and nighttime method (Reichstein et al., 2005) from the EC flux towers, and the remote sensing VIs and meteorological variables (Jung et al., 2017; Tramontana

et al., 2016). The averaged GPP from 6 methods (3 machine learning algorithm × 2 partitioning methods) between 2007 and 2013 were calculated to match the GOME-2 SIF data availability. To compare with the OCO-2 SIF, GPP from 2007 to 2013 were used to calculate the average GPP for the 12 months since these two products do not have overlapping period. This multi-year average can well represent the seasonal dynamic of GPP for each individual year (Fig. S8). Because monthly gridded OCO-2 SIF do not cover the entire global land surface due to the satellite's orbit, we masked the GPP with OCO-2 SIF for the corresponding months before comparison.

To compare the SIF-GPP relationship within each biome type, we aggregated the MODIS MCD12C1 land cover product (https://lpdaac. usgs.gov/dataset_discovery/modis/modis_products_table/mcd12c1) to 0.5° × 0.5° spatial resolution to match with GPP and SIF. For each 0.5° × 0.5° gridcell, we calculated the percentage of each land cover type. Only the gridcells dominated by one land cover type (more than 80%) were considered as "pure" gridcells and used for further analysis (Zhang et al., 2016c). Since the northern hemisphere and southern hemisphere have different growing season, SIF and GPP were averaged within each biome type for each hemisphere.

3. Results

3.1. Comparison between instantaneous GPP and daily GPP at seasonal scale

Fig. 2 shows a comparison between GPP_{daily} and GPP_{inst} at seasonal scale for the Tchizalamousite site in the Congo (CG-Tch) as an example. All GPP_{inst} values at different times of the day (TOD) generally followed the variation of GPP_{daily}, and the γ_{GPP} was also relatively stable across time for TODs between 8:00–16:00 (Fig. 2(a, b)). The regression analysis between GPP_{daily} and GPP_{inst} also showed a similar pattern: TOD with less γ_{GPP} variation exhibited a higher R^2 and the regression slope between GPP_{daily} and GPP_{inst} corresponded to the value of γ_{GPP}. This confirms the feasibility of using regressions between GPP_{daily} and GPP_{inst} to investigate the seasonal and spatial variations of γ_{GPP}.

Using the correlation analysis between GPP_{daily} and GPP_{inst} from all 135 sites at a seasonal scale, we gathered information of the coefficient of determination (R^2) and the regression slopes for each site. For most sites, GPP_{inst} showed a good correlation with GPP_{daily}, especially for GPP_{inst} between 8:00 to 16:00 (Fig. 3a). The correlation was lower for very early morning and late afternoon, but the average R^2 values for these two periods were still higher than 0.8. The regression slopes between GPP_{daily} and GPP_{inst} also varied for different TODs. The averages of regression slopes slightly declined from early morning to midday and increased afterwards. For the period between 8:00 to 16:00 when GPP_{daily} and GPP_{inst} relationships were stronger, the regression slopes also showed less variation.

We also explored the spatial patterns of the regression slopes between GPP_{daily} and GPP_{inst}, by comparing the regression slopes with the cosine of the latitude for each site (Fig. 4). The regression slopes increased from tropical regions (cos(latitude) = 1) to polar regions (cos (latitude) = 0) for most TODs. Between 8:00 to 16:00, the regression slopes between GPP_{daily} and GPP_{inst} can be approximated as a function of cos(latitude), with relatively high R^2 during the midday period (0.81 and 0.87). Biome types did not show much effect on this relationship. Using the analytical approach based on the calculated SZA (Eq. (5)), we obtained the γ_{APAR} at each latitude. The resultant black lines in Fig. 4 generally well-predicted this latitudinal pattern, especially between 8:00 to 16:00. The R^2 between GPP_{daily} and GPP_{inst} also exhibited a latitudinal pattern that could be predicted by the analytical solution of APAR variation (Fig. S2). GPP from daytime and nighttime partitioning methods also exhibited a similar pattern (Figs. S3, S4).

3.2. Comparison between sub-daily instantaneous LUE and daily LUE at seasonal scale

Fig. 5 shows the comparison between the instantaneous LUE and daily LUE for each site at the seasonal scale. Except for the early morning and late afternoon, LUE_{inst} values were generally highly correlated with LUE_{daily}, and this correlation was highest during the middle of the day (10:00–14:00). The regression slopes between LUE_{daily} and LUE_{inst} were also relatively stable for TODs when R^2 values were high. In addition, the slope showed an "U" shape along time with the lowest value being reached during the middle of the day (Fig. 5b). The regression slopes were close to 1 around 10:00 or 14:00, which indicated that the LUE_{inst} at those times can be an approximation of LUE_{daily}.

The difference between the fitted γ_{GPP} curve (red) and simulated γ_{APAR} curve (black) at different TODs in Fig. 4 can be explained by the diurnal change of the LUE_{daily} and LUE_{inst} relationship (γ_{LUE}). This diurnal change of γ_{LUE} is caused by light saturation of GPP as shown in Fig. 6. GPP increases almost linearly with APAR until a light saturating period is reached, when GPP becomes less responsive to radiation (Fig. 6b). This lead to lowest LUE values close to midday, when incident PAR and APAR are the highest (Fig. 6a). The light response curve also suggests that the LUE_{inst} around 9:00 and 15:00 solar time is close to the LUE_{daily}. This explains the overlap of the fitted γ_{GPP} and simulated γ_{APAR} curves during 8:00–10:00 and 14:00–16:00; and the higher γ_{GPP} between 10:00–14:00 over the latitudinal gradient (Fig. 4).

3.3. Comparison between simulated instantaneous and daily SIF from the SCOPE model

To explore whether the instantaneous SIF (SIF_{inst}) and daily SIF (SIF_{daily}) also exhibit a similar latitudinal pattern, we used the SCOPE model and simulated both SIF and GPP for five grassland (or savannas) sites, which cover a wide latitudinal range. The model was run at 30-
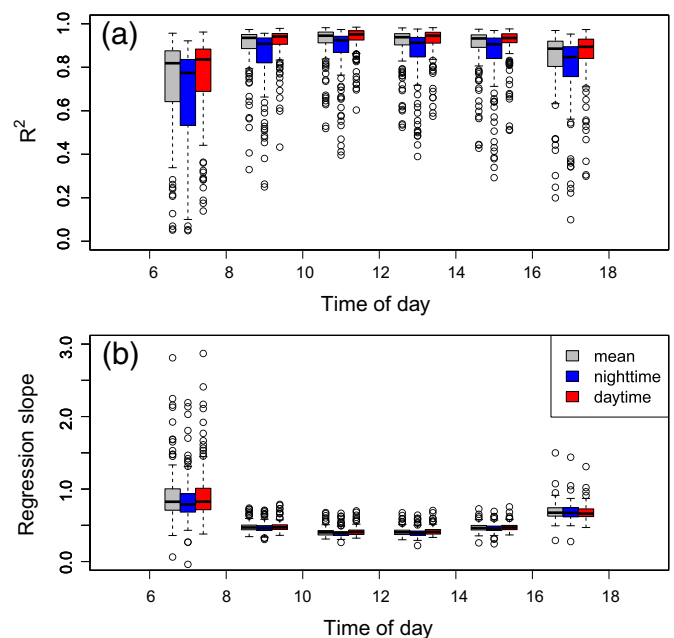

Fig. 3. Boxplots of bi-hourly (a) coefficient of determination (R^2) and (b) linear regression slope between the daily and instantaneous GPP (γ_{GPP}) at seasonal scale across 135 flux tower sites. The linear regressions were forced to pass the origin. Different colors represent GPP estimates from the daytime method (red), nighttime method (blue) or the average of both (grey). The unit of the instantaneous GPP was converted from $\mu mol\ CO_2\ m^{-2}\ s^{-1}$ to $g\ C\ m^{-2}\ day^{-1}$ so that the regression slope is unitless. (For interpretation of the references to color in this figure legend, the reader is referred to the web version of this article.)
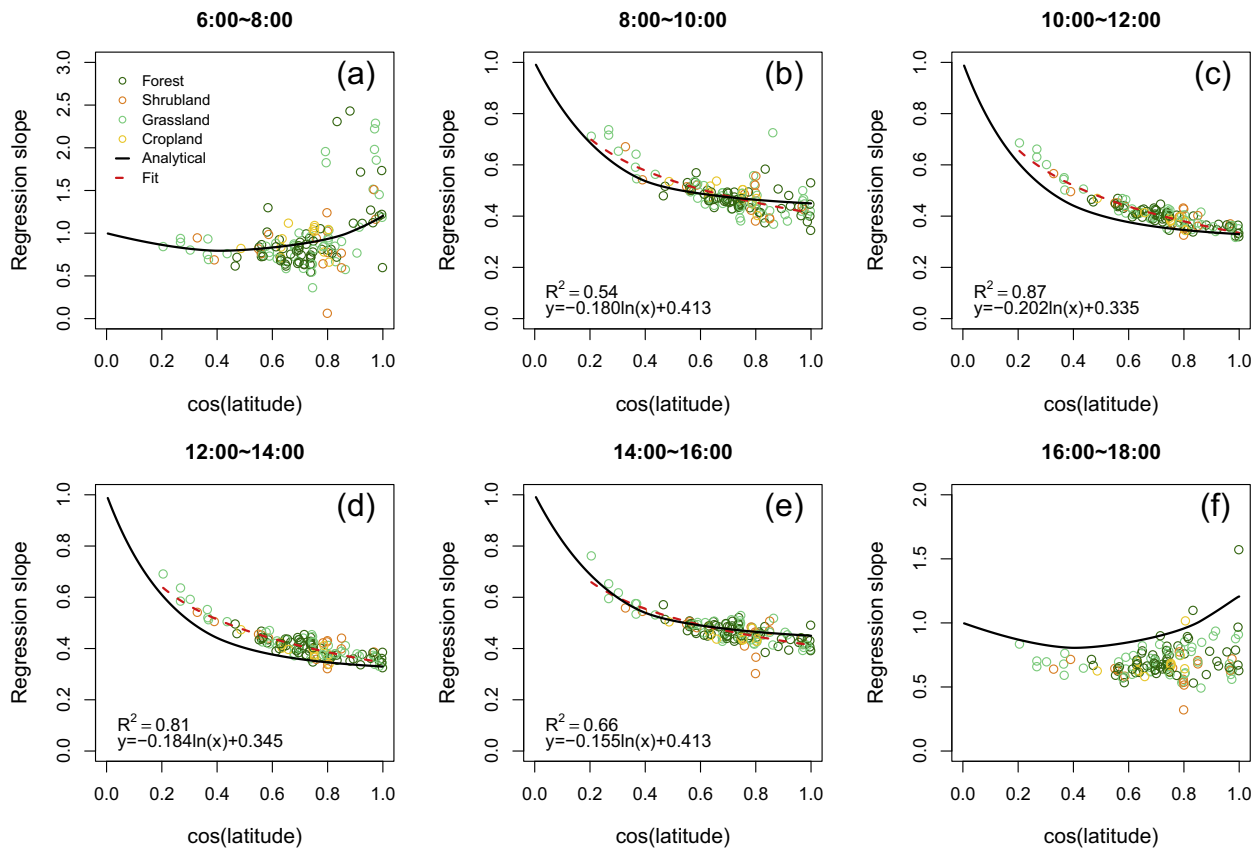
Fig. 4. Latitudinal distribution of regression slopes between daily and instantaneous GPP (γ_{GPP}). GPP from the average of both partitioning methods were used. All biome types (shown in different colors) are aggregated to forest (ENF, EBF, DNF, DBF, MF), shrubland (WSA, OSH, CSH), grassland (GRA, WET, SAV), and cropland (CRO), as shown in different colors. For the full names of the biome types, please refer to the Supplementary information Table S1. Black lines represent the relationship derived from the analytical approximation for γ_{APAR} and cos (latitude). The red dashed lines represent the fitted logarithmic regressions for all sites and not shown in (a) and (f) since the relationship was not significant. (For interpretation of the references to color in this figure legend, the reader is referred to the web version of this article.)
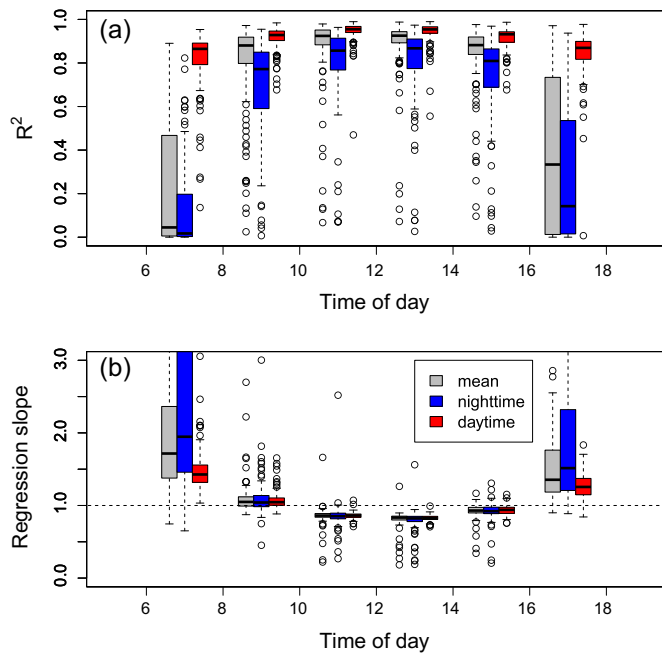

Fig. 5. Comparison between bi-hourly LUE$_{inst}$ and LUE$_{daily}$ across flux tower sites at the seasonal scale. For each site, the correlation and regression slope between LUE$_{daily}$ and LUE$_{inst}$ (γ_{LUE}) at seasonal scale were calculated. Different colors represent GPP estimates from the daytime method (red), nighttime method (blue) or the average of both (grey). (For interpretation of the references to color in this figure legend, the reader is referred to the web version of this article.)

minute intervals for one year to be consistent with the EC data. The simulated GPP and SIF data generally agreed well with the EC tower derived GPP and the SIF retrievals from the GOME-2 instrument (Figs. S5, S6). Most discrepancies were caused by the mismatch of the satellite and flux tower footprints and the uncertainty of LAI or Cab inversions (both the method and the vegetation indices used).

Using the SCOPE model, we found that SIF also followed a similar latitudinal pattern driven by the seasonal variation of PAR. Since we only used one year of data, the γ_{GPP} values for the five sites were sometimes higher than the fitted relationship for some times of day. However, for 8:00–10:00 and 14:00–16:00 when the fitted γ_{GPP} was close to the analytical γ_{APAR}, the regression slopes for simulated SIF from the five sites were close to that of simulated GPP. For 10:00–14:00 when the fitted γ_{GPP} was higher than the analytical γ_{APAR}, the regression slopes for simulated GPP were also higher than those of simulated SIF. Unlike GPP, which has a light saturation period that makes the fitted γ_{GPP} deviate from the γ_{APAR} during the midday, SIF did not show much light saturation and directly followed the γ_{APAR} latitudinal pattern.

We further compared the relationship between the simulated instantaneous SIF and the daily total GPP at the seasonal scale for these five sites (Fig. 8). The linear relationships between GPP and SIF were usually stronger at midday for low to mid-latitude sites, i.e., CG-Tch, US-Var, DK-Eng. But this advantage was not evident for higher latitude sites (DK-ZaH). The daily total SIF and daily total GPP had the highest correlation for both C3 and C4 sites. For C3 sites (all sites except CG-Tch), the regression slopes for SIF and GPP exhibited a smaller variation for early morning and late afternoon (CV = 0.18 and 0.12 for 6:00–8:00 and 16:00–18:00, respectively). While during midday, the
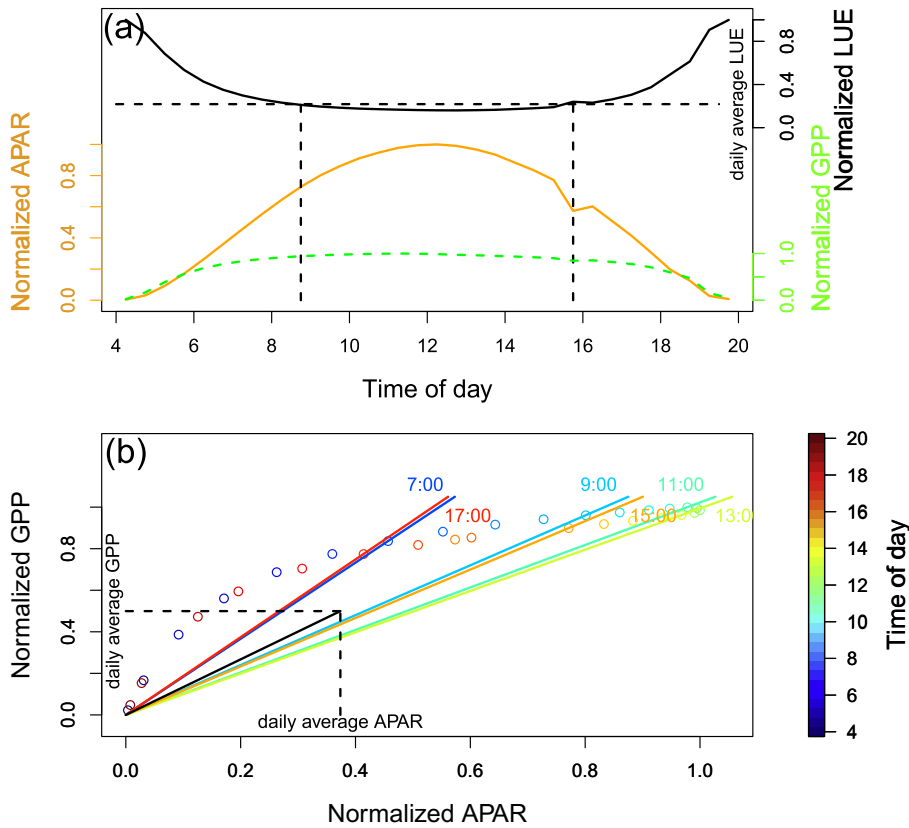
Fig. 6. (a) Dynamic of sub-daily GPP, APAR, and LUE, and (b) the relationship between APAR and GPP at sub-daily scale. One clear day (June 13th, 2014) of data from the US-WCr site is used as an example. The GPP is estimated from the daytime (light response curve) method. All the indicators are normalized by their maximum values. The two vertical dashed lines in (a) indicate the time at which LUE_{inst} equals to LUE_{daily}. The slopes of the solid lines in (b) represent LUE_{inst} ($GPP_{inst}^{normalized}/APAR_{inst}^{normalized}$) at different times of the day and LUE_{daily}.

variation was larger (CV = 0.31 and 0.27 for 10:00–12:00 and 12:00–14:00, respectively). When comparing SIF_{daily} with GPP_{daily}, the regression slopes for all C3 vegetation sites tended to converge to a constant value (0.066, CV = 0.10).

3.4. GPP-SIF comparison at global scale

Fig. 9 shows the comparison between SIF_{inst} or SIF_{daily} with GPP from FluxCom. SIF_{inst} are from direct observations from GOME-2 and OCO-2, while SIF_{daily} values are from analytical approximation using Eq. (7). The SIF_{daily} showed a slightly higher linear correlation (R^2 = 0.94 ± 0.08 for GOME-2 and R^2 = 0.90 ± 0.20 for OCO-2) with GPP than SIF_{inst} (R^2 = 0.92 ± 0.11 for GOME-2 and R^2 = 0.85 ± 0.25 for OCO-2). Except savannas in the southern hemisphere for GOME-2 (0.963 vs. 0.961), all other biome types' coefficient of determination are higher for SIF_{daily} than SIF_{inst}. In addition, the regression slopes among all the biome types for both hemispheres had smaller variation for SIF_{daily} than SIF_{inst}. The use of SIF_{daily} rather than SIF_{inst} showed better improvement of the GPP-SIF relationship for OCO-2 than for GOME-2. Although the comparison between GPP and OCO-2 SIF are from different years, it is expected to have limited effect on our results as the year-to-year variation could be ignored for most biome types (Fig. S8).

4. Discussion

4.1. The relationship between daily GPP and instantaneous SIF across space and time

The spatial and seasonal relationship between GPP_{daily} and satellite observed SIF_{inst} is complicated because both SIF and GPP are driven by solar radiation and have diurnal and seasonal cycles. In this study, using data from multiple flux tower sites, which cover a large spatial extent, we investigated the key issues for estimating spatial and

seasonal GPP dynamics using satellite-retrieved SIF signals.

To link GPP_{daily} with SIF_{inst}, we use:

$$\frac{GPP_{daily}}{SIF_{inst}} = \frac{APAR_{daily} \times LUE_{daily}}{APAR_{inst} \times FE_{inst}} = \frac{APAR_{daily}}{APAR_{inst}} \times \frac{LUE_{daily}}{LUE_{inst}} \times \frac{LUE_{inst}}{FE_{inst}}$$
$$= \gamma_{APAR} \times \gamma_{LUE} \times \frac{LUE_{inst}}{FE_{inst}} \tag{8}$$

In our study, we have demonstrated that the γ_{APAR} is related to the latitude, which is controlled by the seasonal change of day length. As the latitude increases from tropical to polar regions, the day length during the growing season also increases. The instantaneous PAR observation will be close to the average daily PAR during the polar daytime (during the peak growing season in summer), but will be much larger when sun only illuminates for half of the day. We also demonstrated that the variation of γ_{LUE} is related to the observation time mostly caused by the light saturation of photosynthesis and midday depression. The midday depression can be found in some low latitude sites (cos(latitude) ≈ 0.8) where the estimated R^2 for GPP_{inst}-GPP_{daily} deviates from the R^2 predicted with PAR during the midday (10:00–14:00), indicating γ_{GPP} at midday may have higher variation throughout the growing season (Fig. S2). However, this midday variability does not have much effects on the GPP_{inst}-GPP_{daily} regression slopes (Fig. 4). The combination of $\gamma_{APAR} \times \gamma_{LUE}$ can explain the latitudinal and diurnal pattern of the GPP_{daily}-GPP_{inst} relationship. For a specific satellite, we do not need to take γ_{LUE} into consideration as the observation time is often stable (except for the Polar Regions where multiple observations may be obtained within one day), but the latitudinal pattern of γ_{APAR} still needs to be considered. However, when comparing GPP with SIF data from different satellites, the observation time will affect the γ_{LUE} and needs to be taken into account. This means that the GPP-SIF relationship derived from one satellite cannot be directly applied to another if the overpass times of the satellites are different.

Simulations using the SCOPE model suggest that γ_{SIF} tends to follow

γ_{APAR} during midday (Fig. 7). This is consistent with the relatively stable fluorescence yield (ϕ_F) under high light intensity found in previous studies (Lee et al., 2015; van der Tol et al., 2014). But a larger variation of ϕ_F may occur during the shift from low to high irradiance, i.e., when the non-photochemical quenching begins to take effect and the negative correlation between ϕ_F and ϕ_P shifts to positive (Porcar-Castell et al., 2014). The relatively stable ϕ_F under high light intensity can also explain the higher GPP-SIF correlation during midday (10:00–14:00) than early morning or late afternoon for low latitude sites (Fig. 8). However, this advantage is not evident for higher latitude sites, where the growing season in summer is characterized by a very long daytime length and PAR is already/still high at 6:00–8:00 and 16:00–18:00. The regression slopes between GPP$_{daily}$ and SIF$_{inst}$ also had relatively larger variations for midday than early morning or late afternoon, which may be related to the light saturation: lower latitude sites are more likely to be light-saturated during the midday than higher latitude sites. It should also be noted that current version of the SCOPE model did not consider the relationship between nitrogen content (or chlorophyll $a + b$) and maximum carboxylation rate (V_{cmax}) (Ollinger et al., 2008; van der Tol et al., 2009b), therefore the GPP-SIF relationship may be better evaluated with a variable V_{cmax} value. We conducted some preliminary analysis using a variable V_{cmax} that is linearly correlated with Cab. The V_{cmax} was allowed to drop to 50% of its maximum value when Cab was at its minimum. We reproduced Fig. 8 with this variable V_{cmax} settings (Fig. S9), but the results were very similar: high linear correlation were still found when comparing GPP$_{daily}$ with SIF$_{daily}$.

The relationships between LUE$_{inst}$ and fluorescence efficiency (FE$_{inst}$, includes the information of both ϕ_f and the escape coefficient) are still unclear at the seasonal and spatial scale (Porcar-Castell et al., 2014). Recent modeling studies suggested a nonlinear SIF-GPP

relationship at half-hour scale and a strong linear relationship at daily and 16-day scale (Damm et al., 2015; Zhang et al., 2016a). Our comparison between the GOME-2 SIF and FluxCom GPP also showed higher correlation when using the SIF$_{daily}$ value. The variations of the regression slopes across biome types may be related to the C3–C4 species composition (Guan et al., 2016; Liu et al., 2017), average cloud cover during the growing season which affects the direct/diffuse radiation (Gu et al., 2002), canopy characteristics which affect the energy partitioning in different layers and SIF re-absorption (Damm et al., 2015; Migliavacca et al., 2017), and environmental limitations of photosynthesis (temperature, water, etc.) (Ac et al., 2015; van der Tol et al., 2014). These factors together with the latitudinal pattern need to be taken into account when interpreting the relationship between the satellite-based SIF$_{inst}$ and GPP$_{daily}$ at spatial and seasonal scales. In addition, since the midday SIF signal is stronger and the FE$_{inst}$ is more stable and close to the daily average, satellites SIF$_{inst}$ observations with a midday overpass time may have a more linear relationship with GPP$_{daily}$ than those with a morning or afternoon overpass (Fig. 10). However, it should still be noted that the GPP-SIF relationship is affected by the canopy architecture (leaf angle distribution, leaf clumping) but is considered invariant in our simulation. We also tested the SCOPE simulation using other leaf angle distributions (e.g., planophile, erectphile), but the results are similar (data not shown). Some recent studies suggest that 3-dimension canopy structure can be important for canopy energy and carbon fluxes simulations for grass-tree mixed ecosystems (Kobayashi et al., 2012). A more comprehensive representation of 3-dimension canopy structure needs to be incorporated into the SCOPE model to further investigate the effect of canopy structure on SIF-GPP relationship.
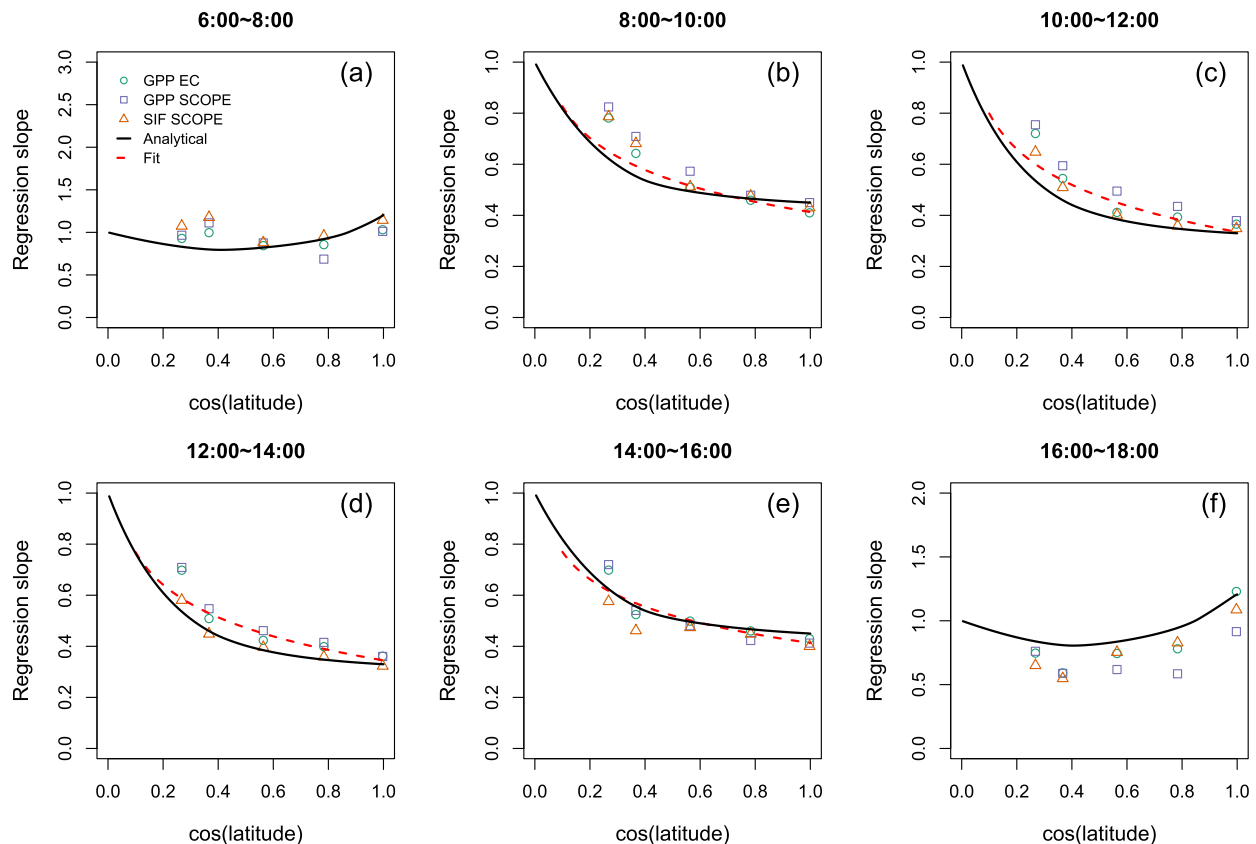

Fig. 7. Latitudinal pattern of regression slopes between daily and instantaneous SCOPE simulated GPP, SIF, and GPP derived from EC tower (open circles). Only one year of data is used (Fig. S5). The red dashed line is from the fitted relationship between daily and instantaneous GPP from EC towers as shown in Fig. 4. The black lines represent the γ_{APAR} from the analytical estimation. (For interpretation of the references to color in this figure legend, the reader is referred to the web version of this article.)
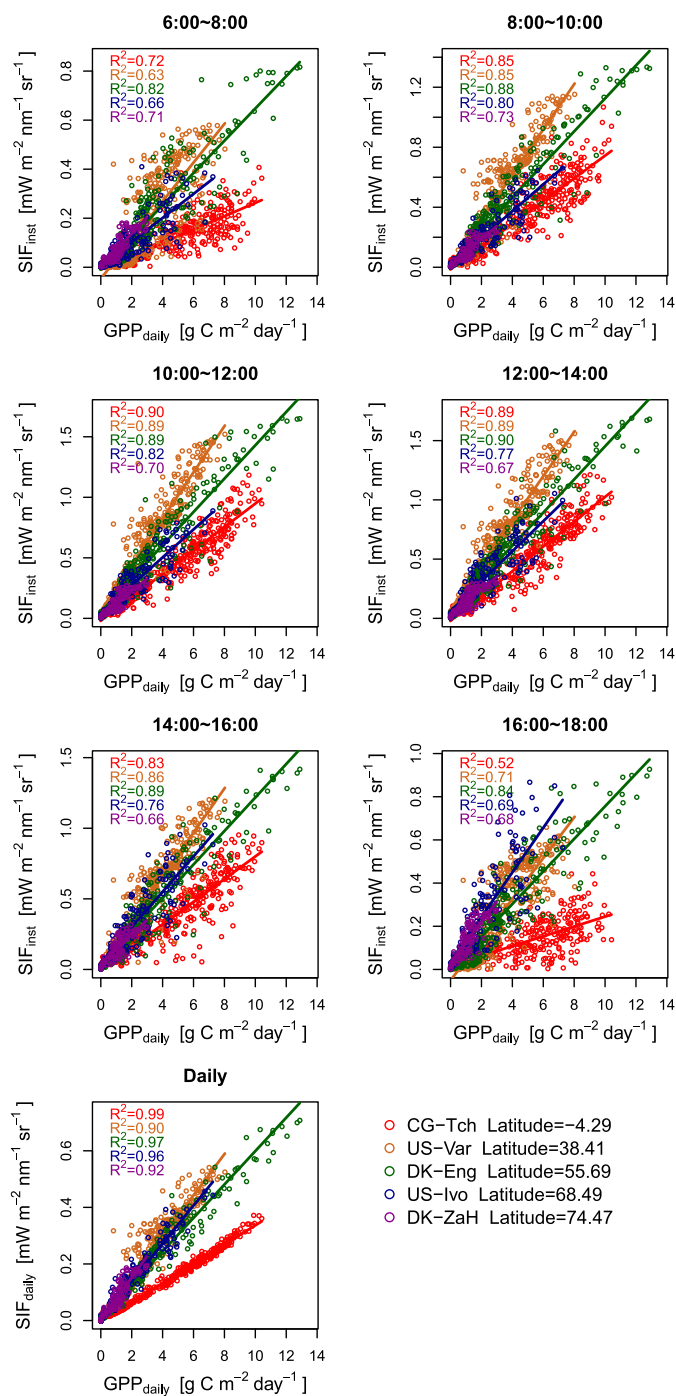
Fig. 8. Scatter diagrams showing the relationship between the instantaneous (upper panels) and daily (bottommost panel) SIF with daily GPP as computed with the SCOPE model for the five sites (color coded) as indicated in the legend. The solid lines with different colors represent the linear regression between SIF and GPP. (For interpretation of the references to color in this figure legend, the reader is referred to the web version of this article.)

4.2. Potential uncertainty for phenological analysis using GOME-2 SIF

As SIF is a measure of energy and has strong diurnal variations, the interpretation of SIF signals at seasonal scale should also be taken with caution. This is directly related to phenology studies, which used SIF as an indicator of vegetation activity (Jeong et al., 2017; Joiner et al., 2014; Walther et al., 2016). Previous phenology studies either used leaf/canopy development or seasonal change of plant physiological properties (e.g., GPP, APAR, termed as "physiological phenology")

(Migliavacca et al., 2015; Piao et al., 2006; Wu et al., 2013; Zhou et al., 2016). The physiological phenology, being different from conventional phenology definition of leaf development or flowering time, is more related to the ecosystem carbon fluxes that directly controlled by plant physiology. The leaf/canopy development measurement can either come from in situ observations (Fu et al., 2015) or satellite-based VIs (Zhang et al., 2003). For the satellite-based VI studies, the start of the growing season is usually determined by detecting the maximum change of rate of VI (second order derivative equals to zero) (Wang et al., 2015; Wu and Liu, 2013; Zhang et al., 2013), or using a threshold (Cong et al., 2013; Zhang et al., 2016b). Since VIs have little diurnal variation, the VIs obtained from different overpass times on a seasonal course can be regarded as the seasonal vegetation growth. In contrast, SIF is a measurement of the energy, and its seasonal variation is controlled by both the seasonal variation of incoming solar radiation, the leaf phenology (fraction of energy being absorbed) and the photosynthetic physiology (fraction of light being emitted as SIF). The contribution from solar radiation is higher at high latitude since PAR at a specific time of day also has large seasonal variations. Therefore, phenology derived from satellite-based SIF measurements cannot be directly compared with phenology derived from VI measurements unless SIF is properly normalized by SZA or instantaneous PAR.

Another question is whether SIF-based phenology can be comparable with GPP or net ecosystem exchange (NEE) based phenology (physiological phenology)? As concluded above, daily SIF has a strong linear relationship with daily GPP within each specific site and should have an advantage over VI at high latitude evergreen ecosystems. When doing phenology analysis, each pixel is analyzed in the temporal domain therefore the latitudinal pattern of instantaneous to daily conversion can be ignored. Then the question becomes whether the conversion from the SIF_{inst} to SIF_{daily} is stable across seasons? Fig. 11(a) shows that the correction factor for GOME-2 and OCO-2 overpass time is not stable even during the growing season for the site US-Ivo. This correction factor has larger variations at higher latitudes, and differs for different satellite overpass times, which may explain the different phenology retrievals of using GOME-2 SIF and GOSAT SIF for boreal forest (Jeong et al., 2017).

To reconcile the discrepancy between SIF and VI observations (Walther et al., 2016), we can either calculate the SIF normalized by the incoming solar radiation at the satellite overpass, represented by the cosine of the solar zenith angle (cos(SZA)). SIF/cos(SZA) will be a measure of fPAR × FE_{inst} and can be used for leaf/greenness based phenology estimation. Alternatively, we can convert the satellite measured SIF_{inst} to SIF_{daily} using Eq. (7), which will be closely linked to the daily GPP. This will give another robust estimation of the photosynthetically active period that can be compared with site level gas exchange data. However, it should be noted that many studies show that fPAR also has a diurnal variation which is related to the SZA, ratios of diffuse to total radiation, and LAI (Chen, 1996; Nouvellon et al., 2000), this may affect the SIF_{inst} to SIF_{daily} conversion using this SZA approximation method as well as the GPP_{inst}-GPP_{daily} relationship. Nevertheless, fPAR is usually found to be higher in early morning or the late afternoon when PAR is low; the product of fPAR and PAR during those times will have limited contribution to daily total APAR and GPP. In addition, as most satellites that can retrieve SIF signals have an overpass close to midday, when the fPAR is relatively stable, SIF_{inst} is also considered less affected by the diurnal variation of fPAR.

5. Conclusions

As satellite observations are often snapshots of the vegetation activity, the usage of satellite observations to infer vegetation activity at seasonal and spatial scales needs to be treated with caution, especially for energy-based measurements such as SIF that exhibit a large diurnal variation. Analyzing data from 135 flux tower sites, we found that both spatial and diurnal patterns exist between daily and instantaneous (bi-
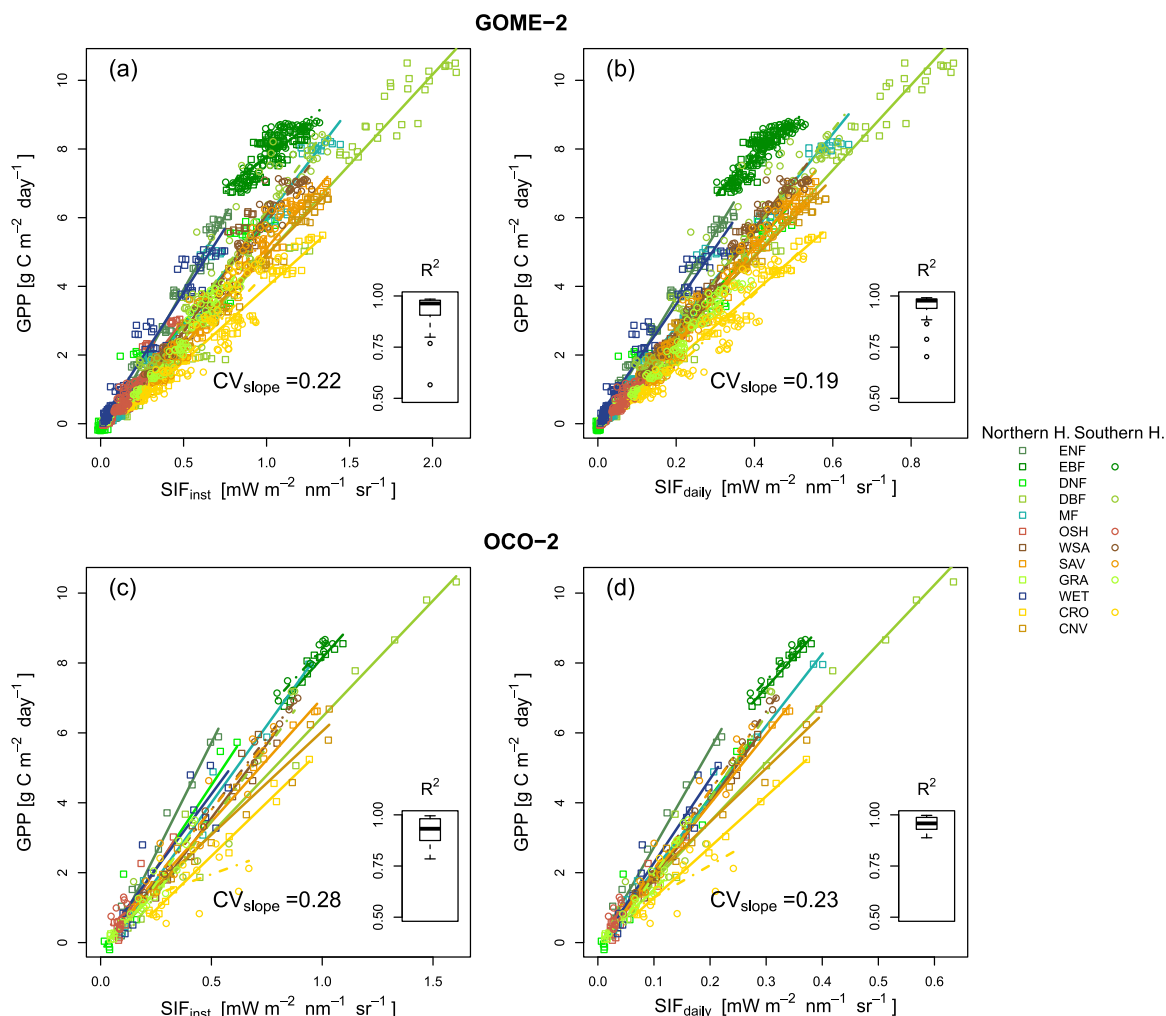
GOME-2

OCO-2

Fig. 9. Comparison between SIF$_{inst}$ and SIF$_{daily}$ from GOME-2 (a, b) and OCO-2 (c, d) with GPP from FluxCom. Only the biome types with more than 100 gridcells were analyzed. Each point represents the average of SIF or GPP for all the gridcells within this biome type for each month for northern or southern hemisphere. For GOME-2, altogether 84 months are used; for OCO-2, 12 months are used (see Materials and method). The solid lines represent the linear regression for northern hemisphere and the dashed lines represent that for southern hemisphere. The insets show the boxplot of the coefficients for all the regressions. For the full names of the biome type, please refer to the Supplementary information Table S1.
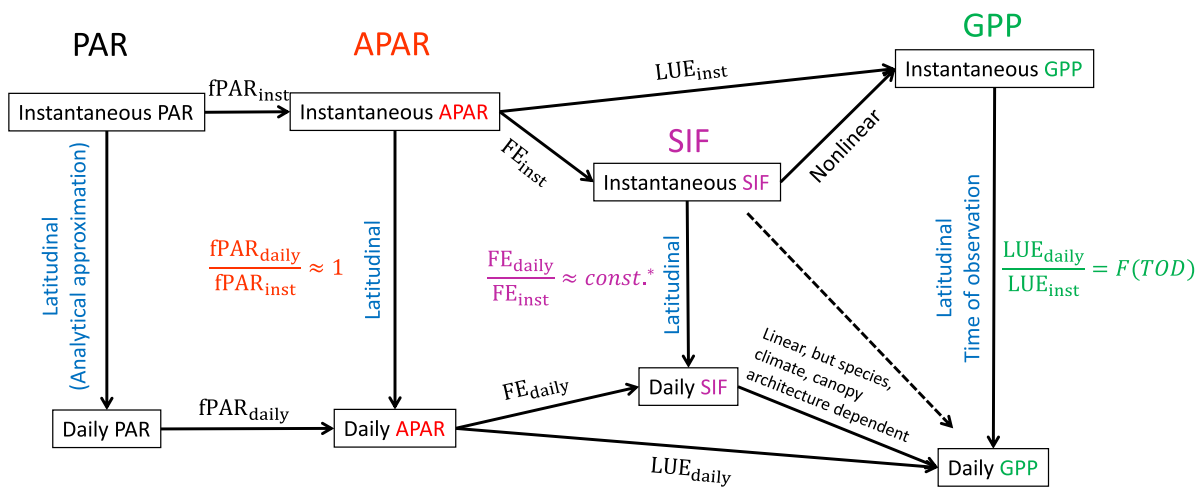

Fig. 10. Schematic diagram showing the relationships between PAR, APAR, SIF and GPP at sub-daily and daily scales. The FE$_{daily}$ and FE$_{inst}$ relationship is close to a constant only under high light intensity, e.g., mid-noon. Solid lines represent that the two variables can be directly linked, while the dashed line represents the relationship cannot be directly established. Abbreviations: PAR: photosynthetically active radiation; APAR: absorbed photosynthetically active radiation; fPAR: fraction of absorbed photosynthetically active radiation; FE: fluorescence efficiency; SIF: solar-induced chlorophyll fluorescence; LUE: light use efficiency; GPP: gross primary production; TOD: time of day.
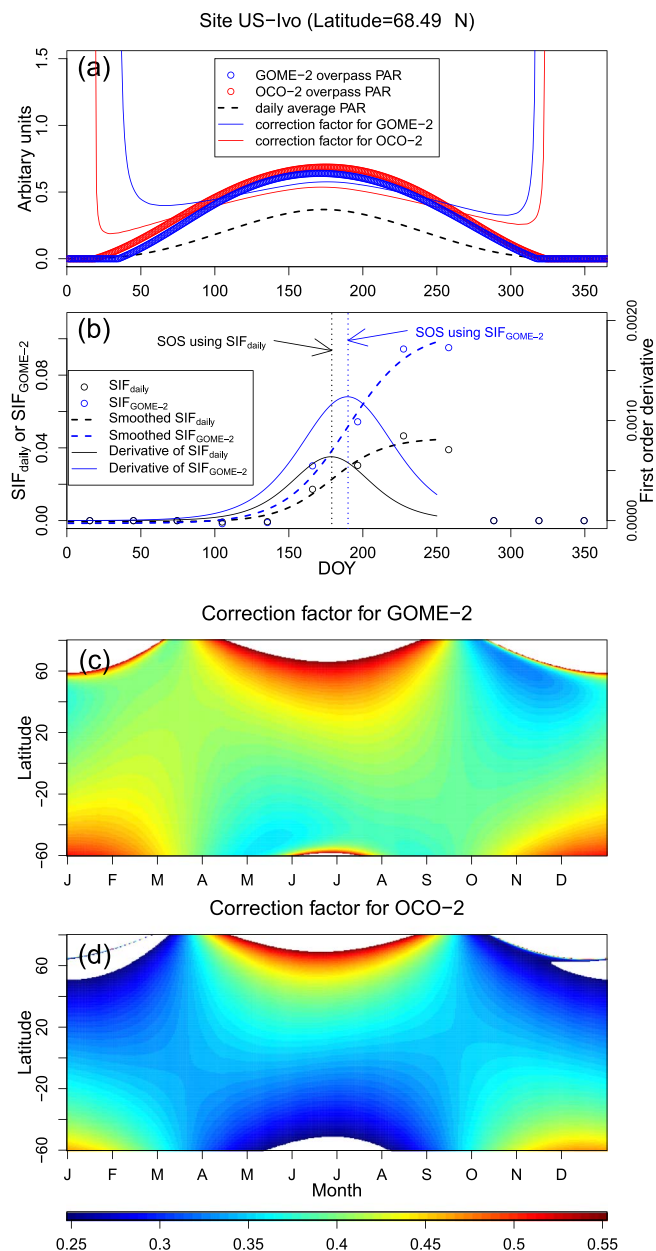
Fig. 11. (a) Relationship between instantaneous PAR at GOME-2 and OCO-2 satellite overpass and the daily average PAR for site US-Ivo (latitude = 68.49˚N). (b) The start of season (SOS) estimates using SIF from both GOME-2 (SIF$_{GOME-2}$) and calculated SIF$_{daily}$. To reduce the relatively high uncertainty in SIF retrieval from one pixel, an average of 5 × 5 pixels were used. The phenology retrieval algorithm is well documented in Joiner et al. (2014) and Zhang et al. (2003). Correction factor for (c) GOME-2 and (d) OCO-2 at different latitude throughout the year. These correction factors were calculated only considering the PAR$_{inst}$-PAR$_{daily}$ relationship.

hourly) GPP. The latitudinal pattern is caused by the variation of PAR and the diurnal pattern is caused by the diurnal variation of LUE.

SIF has shown a high potential to predict GPP across broad spatial and seasonal scales. However, satellite-derived instantaneous SIF retrievals and daily GPP relationships on spatial and seasonal courses are still affected by several factors such as latitude, satellite overpass time, C3/C4 composition, environmental stress, canopy architecture, etc. Using the SCOPE model simulation and the comparison between GOME-2 SIF and FluxCom GPP, we have shown that the relationship between daily average SIF and daily total GPP are more consistent across latitudinal gradients and biome types than those between instantaneous SIF and daily GPP, and the correction factor from

instantaneous to daily SIF improved the linear relationship between satellite-based SIF retrievals and daily GPP. This factor should also be applied when using SIF to derive the physiological phenology. Since this correction factor is based on the analytical approximation of solar zenith angle and does not consider the diurnal variation of other environmental factors (e.g., temperature, water stress), more in situ measurements of SIF are needed at sub-daily time scale for different ecosystems to better interpret the GPP-SIF relationship globally. Canopy architecture that directly affects the energy absorption and partitioning in different layers can be another important issue that warrants further study. The NASA Tropospheric Emissions: Monitoring of Pollution (TEMPO), Geostationary Carbon Cycle Observatory (GeoCARB), as well as European Sentinel 4 missions will provide further valuable insights about the diurnal SIF variation at regional and larger scales.

Appendix A. Supplementary data

Supplementary data to this article can be found online at https://doi.org/10.1016/j.rse.2017.12.009.

References

Ac, A., Malenovsky, Z., Olejnickova, J., Galle, A., Rascher, U., Mohammed, G., 2015. Meta-analysis assessing potential of steady-state chlorophyll fluorescence for remote sensing detection of plant water, temperature and nitrogen stress. Remote Sens. Environ. 168, 420–436.

Anav, A., Friedlingstein, P., Beer, C., Ciais, P., Harper, A., Jones, C., Murray-Tortarolo, G., Papale, D., Parazoo, N.C., Peylin, P., Piao, S., Sitch, S., Viovy, N., Wiltshire, A., Zhao, M., 2015. Spatiotemporal patterns of terrestrial gross primary production: a review. Rev. Geophys. 53, 785–818.

Asrar, G., Kanemasu, E.T., Miller, G.P., Weiser, R., 1986. Light interception and leaf area estimates from measurements of grass canopy reflectance. IEEE Trans. Geosci. Remote Sens. 76–82.

Aubinet, M., Vesala, T., Papale, D., 2012. Eddy Covariance: A Practical Guide to Measurement and Data Analysis. Springer Science & Business Media.

Baker, N.R., 2008. Chlorophyll fluorescence: a probe of photosynthesis in vivo. Annu. Rev. Plant Biol. 59, 89–113.

Baldocchi, D., Falge, E., Gu, L.H., Olson, R., Hollinger, D., Running, S., Anthoni, P., Bernhofer, C., Davis, K., Evans, R., Fuentes, J., Goldstein, A., Katul, G., Law, B., Lee, X.H., Malhi, Y., Meyers, T., Munger, W., Oechel, W., U, K.T.P., Pilegaard, K., Schmid, H.P., Valentini, R., Verma, S., Vesala, T., Wilson, K., Wofsy, S., 2001. FLUXNET: a new tool to study the temporal and spatial variability of ecosystem-scale carbon dioxide, water vapor, and energy flux densities. Bull. Am. Meteorol. Soc. 82, 2415–2434.

Barr, A., Richardson, A., Hollinger, D., Papale, D., Arain, M., Black, T., Bohrer, G., Dragoni, D., Fischer, M., Gu, L., 2013. Use of change-point detection for

friction–velocity threshold evaluation in eddy-covariance studies. Agric. For. Meteorol. 171, 31–45.

Beer, C., Reichstein, M., Tomelleri, E., Ciais, P., Jung, M., Carvalhais, N., Rödenbeck, C., Arain, M.A., Baldocchi, D., Bonan, G.B., 2010. Terrestrial gross carbon dioxide up-take: global distribution and covariation with climate. Science 329, 834–838.

Bi, J., Knyazikhin, Y., Choi, S., Park, T., Barichivich, J., Ciais, P., Fu, R., Ganguly, S., Hall, F., Hilker, T., Huete, A., Jones, M., Kimball, J., Lyapustin, A.I., Mõttus, M., Nemani, R.R., Piao, S., Poulter, B., Saleska, S.R., Saatchi, S.S., Xu, L., Zhou, L., Myneni, R.B., 2015. Sunlight mediated seasonality in canopy structure and photosynthetic activity of Amazonian rainforests. Environ. Res. Lett. 10, 064014.

Chen, J.M., 1996. Canopy architecture and remote sensing of the fraction of photo-synthetically active radiation absorbed by boreal conifer forests. IEEE Trans. Geosci. Remote Sens. 34, 1353–1368.

Cong, N., Wang, T., Nan, H., Ma, Y., Wang, X., Myneni, R.B., Piao, S., 2013. Changes in satellite-derived spring vegetation green-up date and its linkage to climate in China from 1982 to 2010: a multimethod analysis. Glob. Chang. Biol. 19, 881–891.

Damm, A., Elbers, J., Erler, A., Gioli, B., Hamdi, K., Hutjes, R., Kosvancova, M., Meroni, M., Miglietta, F., Moersch, A., Moreno, J., Schickling, A., Sonnenschein, R., Udelhoven, T., van der Linden, S., Hostert, P., Rascher, U., 2010. Remote sensing of sun-induced fluorescence to improve modeling of diurnal courses of gross primary production (GPP). Glob. Chang. Biol. 16, 171–186.

Damm, A., Guanter, L., Paul-Limoges, E., van der Tol, C., Hueni, A., Buchmann, N., Eugster, W., Ammann, C., Schaepman, M.E., 2015. Far-red sun-induced chlorophyll fluorescence shows ecosystem-specific relationships to gross primary production: an assessment based on observational and modeling approaches. Remote Sens. Environ. 166, 91–105.

Dash, J., Curran, P.J., 2004. The MERIS terrestrial chlorophyll index. Int. J. Remote Sens. 25, 5403–5413.

Farquhar, G.D., Caemmerer, S.V., Berry, J.A., 1980. A biochemical-model of photo-synthetic CO_2 assimilation in leaves of C-3 species. Planta 149, 78–90.

Fensholt, R., Sandholt, I., Rasmussen, M.S., 2004. Evaluation of MODIS LAI, fAPAR and the relation between fAPAR and NDVI in a semi-arid environment using in situ measurements. Remote Sens. Environ. 91, 490–507.

Frankenberg, C., 2015. In: C.I.o. Technology (Ed.), Solar Induced Chlorophyll Fluorescence OCO-2 Lite Files (B7000) User Guide.

Frankenberg, C., Fisher, J.B., Worden, J., Badgley, G., Saatchi, S.S., Lee, J.E., Toon, G.C., Butz, A., Jung, M., Kuze, A., Yokota, T., 2011. New global observations of the ter-restrial carbon cycle from GOSAT: patterns of plant fluorescence with gross primary productivity. Geophys. Res. Lett. 38.

Frankenberg, C., O'Dell, C., Berry, J., Guanter, L., Joiner, J., Köhler, P., Pollock, R., Taylor, T.E., 2014. Prospects for chlorophyll fluorescence remote sensing from the Orbiting Carbon Observatory-2. Remote Sens. Environ. 147, 1–12.

Fu, Y.H., Zhao, H., Piao, S., Peaucelle, M., Peng, S., Zhou, G., Ciais, P., Huang, M., Menzel, A., Peñuelas, J., Song, Y., Vitasse, Y., Zeng, Z., Janssens, I.A., 2015. Declining global warming effects on the phenology of spring leaf unfolding. Nature 526, 104–107.

Genty, B., Briantais, J.-M., Baker, N.R., 1989. The relationship between the quantum yield of photosynthetic electron transport and quenching of chlorophyll fluorescence. Biochim. Biophys. Acta Gen. Subj. 990, 87–92.

Gu, L., Baldocchi, D., Verma, S.B., Black, T.A., Vesala, T., Falge, E.M., Dowty, P.R., 2002. Advantages of diffuse radiation for terrestrial ecosystem productivity. J. Geophys. Res. Atmos. 107 (ACL 2-1–ACL 2-23).

Guan, K., Pan, M., Li, H., Wolf, A., Wu, J., Medvigy, D., Caylor, K.K., Sheffield, J., Wood, E.F., Malhi, Y., Liang, M., Kimball, J.S., Saleska, Scott R., Berry, J., Joiner, J., Lyapustin, A.I., 2015. Photosynthetic seasonality of global tropical forests con-strained by hydroclimate. Nat. Geosci. 8, 284–289.

Guan, K., Berry, J.A., Zhang, Y., Joiner, J., Guanter, L., Badgley, G., Lobell, D.B., 2016. Improving the monitoring of crop productivity using spaceborne solar-induced fluorescence. Glob. Chang. Biol. 22, 716–726.

Guanter, L., Zhang, Y., Jung, M., Joiner, J., Voigt, M., Berry, J.A., Frankenberg, C., Huete, A.R., Zarco-Tejada, P., Lee, J.E., Moran, M.S., Ponce-Campos, G., Beer, C., Camps-Valls, G., Buchmann, N., Gianelle, D., Klumpp, K., Cescatti, A., Baker, J.M., Griffis, T.J., 2014. Global and time-resolved monitoring of crop photosynthesis with chlor-ophyll fluorescence. Proc. Natl. Acad. Sci. U. S. A 111, E1327–1333.

Guanter, L., Aben, I., Tol, P., Krijger, J.M., Hollstein, A., Kohler, P., Damm, A., Joiner, J., Frankenberg, C., Landgraf, J., 2015. Potential of the TROPOspheric Monitoring Instrument (TROPOMI) onboard the Sentinel-5 Precursor for the monitoring of ter-restrial chlorophyll fluorescence. Atmos. Meas. Tech. 8, 1337–1352.

Huete, A.R., Didan, K., Shimabukuro, Y.E., Ratana, P., Saleska, S.R., Hutyra, L.R., Yang, W., Nemani, R.R., Myneni, R., 2006. Amazon rainforests green-up with sunlight in dry season. Geophys. Res. Lett. 33.

Jeong, S.-J., Schimel, D., Frankenberg, C., Drewry, D.T., Fisher, J.B., Verma, M., Berry, J.A., Lee, J.-E., Joiner, J., 2017. Application of satellite solar-induced chlorophyll fluorescence to understanding large-scale variations in vegetation phenology and function over northern high latitude forests. Remote Sens. Environ. 190, 178–187.

Joiner, J., Yoshida, Y., Vasilkov, A.P., Middleton, E.M., Campbell, P.K.E., Yoshida, Y., Kuze, A., Corp, L.A., 2012. Filling-in of near-infrared solar lines by terrestrial fluor-escence and other geophysical effects: simulations and space-based observations from SCIAMACHY and GOSAT. Atmos. Meas. Tech. 5, 809–829.

Joiner, J., Guanter, L., Lindstrot, R., Voigt, M., Vasilkov, A.P., Middleton, E.M., Huemmrich, K.F., Yoshida, Y., Frankenberg, C., 2013. Global monitoring of terrestrial chlorophyll fluorescence from moderate-spectral-resolution near-infrared satellite measurements: methodology, simulations, and application to GOME-2. Atmos. Meas. Tech. 6, 2803–2823.

Joiner, J., Yoshida, Y., Vasilkov, A.P., Schaefer, K., Jung, M., Guanter, L., Zhang, Y., Garrity, S., Middleton, E.M., Huemmrich, K.F., Gu, L., Belelli Marchesini, L., 2014. The seasonal cycle of satellite chlorophyll fluorescence observations and its

relationship to vegetation phenology and ecosystem atmosphere carbon exchange. Remote Sens. Environ. 152, 375–391.

Joiner, J., Yoshida, Y., Guanter, L., Middleton, E., 2016. New methods for retrieval of chlorophyll red fluorescence from hyper-spectral satellite instruments: simulations and application to GOME-2 and SCIAMACHY. Atmos. Meas. Tech. 9, 3939–3967.

Jung, M., Reichstein, M., Schwalm, C.R., Huntingford, C., Sitch, S., Ahlstrom, A., Arneth, A., Camps-Valls, G., Ciais, P., Friedlingstein, P., Gans, F., Ichii, K., Jain, A.K., Kato, E., Papale, D., Poulter, B., Raduly, B., Rodenbeck, C., Tramontana, G., Viovy, N., Wang, Y.P., Weber, U., Zaehle, S., Zeng, N., 2017. Compensatory water effects link yearly global land CO_2 sink changes to temperature. Nature 541, 516–520.

Kattge, J., Knorr, W., Raddatz, T., Wirth, C., 2009. Quantifying photosynthetic capacity and its relationship to leaf nitrogen content for global-scale terrestrial biosphere models. Glob. Chang. Biol. 15, 976–991.

Kobayashi, H., Baldocchi, D.D., Ryu, Y., Chen, Q., Ma, S., Osuna, J.L., Ustin, S.L., 2012. Modeling energy and carbon fluxes in a heterogeneous oak woodland: a three-di-mensional approach. Agric. For. Meteorol. 152, 83–100.

Krause, G., Weis, E., 1991. Chlorophyll fluorescence and photosynthesis: the basics. Annu. Rev. Plant Biol. 42, 313–349.

Lasslop, G., Reichstein, M., Papale, D., Richardson, A.D., Arneth, A., Barr, A., Stoy, P., Wohlfahrt, G., 2010. Separation of net ecosystem exchange into assimilation and respiration using a light response curve approach: critical issues and global evalua-tion. Glob. Chang. Biol. 16, 187–208.

Lee, J.E., Berry, J.A., van der Tol, C., Yang, X., Guanter, L., Damm, A., Baker, I., Frankenberg, C., 2015. Simulations of chlorophyll fluorescence incorporated into the Community Land Model version 4. Glob. Chang. Biol. 21, 3469–3477.

Liu, L., Guan, L., Liu, X., 2017. Directly estimating diurnal changes in GPP for C3 and C4 crops using far-red sun-induced chlorophyll fluorescence. Agric. For. Meteorol. 232, 1–9.

Los, S.O., North, P.R.J., Grey, W.M.F., Barnsley, M.J., 2005. A method to convert AVHRR Normalized Difference Vegetation Index time series to a standard viewing and illu-mination geometry. Remote Sens. Environ. 99, 400–411.

Luo, Y., Ogle, K., Tucker, C., Fei, S., Gao, C., LaDeau, S., Clark, J.S., Schimel, D.S., 2011. Ecological forecasting and data assimilation in a data-rich era. Ecol. Appl. 21, 1429–1442.

Migliavacca, M., Reichstein, M., Richardson, A.D., Mahecha, M.D., Cremonese, E., Delpierre, N., Galvagno, M., Law, B.E., Wohlfahrt, G., Andrew Black, T., Carvalhais, N., Ceccherini, G., Chen, J., Gobron, N., Koffi, E., William Munger, J., Perez-Priego, O., Robustelli, M., Tomelleri, E., Cescatti, A., 2015. Influence of physiological phe-nology on the seasonal pattern of ecosystem respiration in deciduous forests. Glob. Chang. Biol. 21, 363–376.

Migliavacca, M., Perez-Priego, O., Rossini, M., El-Madany, T.S., Moreno, G., van der Tol, C., Rascher, U., Berninger, A., Bessenbacher, V., Burkart, A., Carrara, A., Fava, F., Guan, J.H., Hammer, T.W., Henkel, K., Juarez-Alcalde, E., Julitta, T., Kolle, O., Martin, M.P., Musavi, T., Pacheco-Labrador, J., Perez-Burgueno, A., Wutzler, T., Zaehle, S., Reichstein, M., 2017. Plant functional traits and canopy structure control the relationship between photosynthetic CO_2 uptake and far-red sun-induced fluor-escence in a Mediterranean grassland under different nutrient availability. New Phytol. 214, 1078–1091.

Monteith, J.L., 1972. Solar-radiation and productivity in tropical ecosystems. J. Appl. Ecol. 9, 747–766.

Morton, D.C., Nagol, J., Carabajal, C.C., Rosette, J., Palace, M., Cook, B.D., Vermote, E.F., Harding, D.J., North, P.R.J., 2014. Amazon forests maintain consistent canopy structure and greenness during the dry season. Nature 506, 221–224.

Nouvellon, Y., Begue, A., Moran, M.S., Lo Seen, D., Rambal, S., Luquet, D., Chehbouni, G., Inoue, Y., 2000. PAR extinction in shortgrass ecosystems: effects of clumping, sky conditions and soil albedo. Agric. For. Meteorol. 105, 21–41.

Ollinger, S.V., Richardson, A.D., Martin, M.E., Hollinger, D.Y., Frolking, S.E., Reich, P.B., Plourde, L.C., Katul, G.G., Munger, J.W., Oren, R., Smithb, M.L., U, K.T.P., Bolstad, P.V., Cook, B.D., Day, M.C., Martin, T.A., Monson, R.K., Schmid, H.P., 2008. Canopy nitrogen, carbon assimilation, and albedo in temperate and boreal forests: functional relations and potential climate feedbacks. Proc. Natl. Acad. Sci. U. S. A. 105, 19336–19341.

Papale, D., Reichstein, M., Aubinet, M., Canfora, E., Bernhofer, C., Kutsch, W., Longdoz, B., Rambal, S., Valentini, R., Vesala, T., 2006. Towards a standardized processing of Net Ecosystem Exchange measured with eddy covariance technique: algorithms and uncertainty estimation. Biogeosciences 3, 571–583.

Pastorello, G.Z., Papale, D., Chu, H., Trotta, C., Agarwal, D.A., Canfora, E., Baldocchi, D.D., Torn, M.S., 2017. A new data set to keep a sharper eye on land-air exchanges. Eos 98. http://dx.doi.org/10.1029/2017EO071597.

Peng, C.H., Guiot, J., Wu, H.B., Jiang, H., Luo, Y.Q., 2011. Integrating models with data in ecology and palaeoecology: advances towards a model-data fusion approach. Ecol. Lett. 14, 522–536.

Piao, S., Fang, J., Zhou, L., Ciais, P., Zhu, B., 2006. Variations in satellite-derived phe-nology in China's temperate vegetation. Glob. Chang. Biol. 12, 672–685.

Porcar-Castell, A., Tyystjarvi, E., Atherton, J., van der Tol, C., Flexas, J., Pfundel, E.E., Moreno, J., Frankenberg, C., Berry, J.A., 2014. Linking chlorophyll a fluorescence to photosynthesis for remote sensing applications: mechanisms and challenges. J. Exp. Bot. 65, 4065–4095.

Reichstein, M., Falge, E., Baldocchi, D., Papale, D., Aubinet, M., Berbigier, P., Bernhofer, C., Buchmann, N., Gilmanov, T., Granier, A., Grunwald, T., Havrankova, K., Ilvesniemi, H., Janous, D., Knohl, A., Laurila, T., Lohila, A., Loustau, D., Matteucci, G., Meyers, T., Miglietta, F., Ourcival, J.-M., Pumpanen, J., Rambal, S., Rotenberg, E., Sanz, M., Tenhunen, J., Seufert, G., Vaccari, F., Vesala, T., Yakir, D., Valentini, R., 2005. On the separation of net ecosystem exchange into assimilation and ecosystem respiration: review and improved algorithm. Glob. Chang. Biol. 11, 1424–1439.

Ryu, Y., Baldocchi, D.D., Black, T.A., Detto, M., Law, B.E., Leuning, R., Miyata, A.,

Reichstein, M., Vargas, R., Ammann, C., Beringer, J., Flanagan, L.B., Gu, L.H., Hutley, L.B., Kim, J., McCaughey, H., Moors, E.J., Rambal, S., Vesala, T., 2012. On the temporal upscaling of evapotranspiration from instantaneous remote sensing measurements to 8-day mean daily-sums. Agric. For. Meteorol. 152, 212–222.

Schimel, D., Pavlick, R., Fisher, J.B., Asner, G.P., Saatchi, S., Townsend, P., Miller, C., Frankenberg, C., Hibbard, K., Cox, P., 2015. Observing terrestrial ecosystems and the carbon cycle from space. Glob. Chang. Biol. 21, 1762–1776.

Sims, D.A., Rahman, A.F., Cordova, V.D., Baldocchi, D.D., Flanagan, L.B., Goldstein, A.H., Hollinger, D.Y., Misson, L., Monson, R.K., Schmid, H.P., Wofsy, S.C., Xu, L.K., 2005. Midday values of gross CO_2 flux and light use efficiency during satellite overpasses can be used to directly estimate eight-day mean flux. Agric. For. Meteorol. 131, 1–12.

Tramontana, G., Jung, M., Schwalm, C.R., Ichii, K., Camps-Valls, G., Raduly, B., Reichstein, M., Arain, M.A., Cescatti, A., Kiely, G., Merbold, L., Serrano-Ortiz, P., Sickert, S., Wolf, S., Papale, D., 2016. Predicting carbon dioxide and energy fluxes across global FLUXNET sites with regression algorithms. Biogeosciences 13, 4291–4313.

van der Tol, C., Verhoef, W., Rosema, A., 2009a. A model for chlorophyll fluorescence and photosynthesis at leaf scale. Agric. For. Meteorol. 149, 96–105.

van der Tol, C., Verhoef, W., Timmermans, J., Verhoef, A., Su, Z., 2009b. An integrated model of soil-canopy spectral radiances, photosynthesis, fluorescence, temperature and energy balance. Biogeosciences 6, 3109–3129.

van der Tol, C., Berry, J.A., Campbell, P.K.E., Rascher, U., 2014. Models of fluorescence and photosynthesis for interpreting measurements of solar-induced chlorophyll fluorescence. J. Geophys. Res. Biogeosci. 119, 2312–2327.

Verma, M., Friedl, M.A., Law, B.E., Bonal, D., Kiely, G., Black, T.A., Wohlfahrt, G., Moors, E.J., Montagnani, L., Marcolla, B., Toscano, P., Varlagin, A., Roupsard, O., Cescatti, A., Arain, M.A., D'Odorico, P., 2015. Improving the performance of remote sensing models for capturing intra- and inter-annual variations in daily GPP: an analysis using global FLUXNET tower data. Agric. For. Meteorol. 214-215, 416–429.

Verrelst, J., Rivera, J.P., van der Tol, C., Magnani, F., Mohammed, G., Moreno, J., 2015. Global sensitivity analysis of the SCOPE model: what drives simulated canopy-leaving sun-induced fluorescence? Remote Sens. Environ. 166, 8–21.

Verrelst, J., van der Tol, C., Magnani, F., Sabater, N., Rivera, J.P., Mohammed, G., Moreno, J., 2016. Evaluating the predictive power of sun-induced chlorophyll fluorescence to estimate net photosynthesis of vegetation canopies: a SCOPE modeling study. Remote Sens. Environ. 176, 139–151.

Vuichard, N., Papale, D., 2015. Filling the gaps in meteorological continuous data measured at FLUXNET sites with ERA-interim reanalysis. Earth Syst. Sci. Data 7, 157.

Wagle, P., Zhang, Y., Jin, C., Xiao, X., 2016. Comparison of solar-induced chlorophyll fluorescence, light-use efficiency, and process-based GPP models in maize. Ecol. Appl. 26, 1211–1222.

Walther, S., Voigt, M., Thum, T., Gonsamo, A., Zhang, Y., Koehler, P., Jung, M., Varlagin, A., Guanter, L., 2016. Satellite chlorophyll fluorescence measurements reveal large-scale decoupling of photosynthesis and greenness dynamics in boreal evergreen forests. Glob. Chang. Biol. 22, 2979–2996.

Wang, X.H., Piao, S.L., Xu, X.T., Ciais, P., MacBean, N., Myneni, R.B., Li, L., 2015. Has the advancing onset of spring vegetation green-up slowed down or changed abruptly over the last three decades? Glob. Ecol. Biogeogr. 24, 621–631.

Wohlfahrt, G., Gu, L., 2015. The many meanings of gross photosynthesis and their implication for photosynthesis research from leaf to globe. Plant Cell Environ. 38, 2500–2507.

Wu, X., Liu, H., 2013. Consistent shifts in spring vegetation green-up date across temperate biomes in China, 1982–2006. Glob. Chang. Biol. 19, 870–880.

Wu, C.Y., Chen, J.M., Black, T.A., Price, D.T., Kurz, W.A., Desai, A.R., Gonsamo, A., Jassal, R.S., Gough, C.M., Bohrer, G., Dragoni, D., Herbst, M., Gielen, B., Berninger, F., Vesala, T., Mammarella, I., Pilegaard, K., Blanken, P.D., 2013. Interannual variability of net ecosystem productivity in forests is explained by carbon flux phenology in autumn. Glob. Ecol. Biogeogr. 22, 994–1006.

Wullschleger, S.D., 1993. Biochemical limitations to carbon assimilation in C3 plants—a retrospective analysis of the A/Ci curves from 109 species. J. Exp. Bot. 44, 907–920.

Yang, X., Tang, J., Mustard, J.F., Lee, J.-E., Rossini, M., Joiner, J., Munger, J.W., Kornfeld, A., Richardson, A.D., 2015. Solar-induced chlorophyll fluorescence correlates with canopy photosynthesis on diurnal and seasonal scales in a temperate deciduous forest. Geophys. Res. Lett. 42, 2977–2987.

Zhang, X.Y., Friedl, M.A., Schaaf, C.B., Strahler, A.H., Hodges, J.C.F., Gao, F., Reed, B.C., Huete, A., 2003. Monitoring vegetation phenology using MODIS. Remote Sens. Environ. 84, 471–475.

Zhang, G., Zhang, Y., Dong, J., Xiao, X., 2013. Green-up dates in the Tibetan Plateau have continuously advanced from 1982 to 2011. Proc. Natl. Acad. Sci. U. S. A. 110, 4309–4314.

Zhang, Y., Guanter, L., Berry, J.A., Joiner, J., van der Tol, C., Huete, A., Gitelson, A., Voigt, M., Kohler, P., 2014. Estimation of vegetation photosynthetic capacity from space-based measurements of chlorophyll fluorescence for terrestrial biosphere models. Glob. Chang. Biol. 20, 3727–3742.

Zhang, Y., Guanter, L., Berry, J.A., van der Tol, C., Yang, X., Tang, J., Zhang, F., 2016a. Model-based analysis of the relationship between sun-induced chlorophyll fluorescence and gross primary production for remote sensing applications. Remote Sens. Environ. 187, 145–155.

Zhang, Y., Peng, C., Li, W., Tian, L., Zhu, Q., Chen, H., Fang, X., Zhang, G., Liu, G., Mu, X., Li, Z., Li, S., Yang, Y., Wang, J., Xiao, X., 2016b. Multiple afforestation programs accelerate the greenness in the 'Three North' region of China from 1982 to 2013. Ecol. Indic. 61, 404–412.

Zhang, Y., Xiao, X., Guanter, L., Zhou, S., Ciais, P., Joiner, J., Sitch, S., Wu, X., Nabel, J., Dong, J., Kato, E., Jain, A.K., Wiltshire, A., Stocker, B.D., 2016c. Precipitation and carbon-water coupling jointly control the interannual variability of global land gross primary production. Sci. Rep. 6, 39748.

Zhang, Y., Xiao, X., Jin, C., Dong, J., Zhou, S., Wagle, P., Joiner, J., Guanter, L., Zhang, Y., Zhang, G., Qin, Y., Wang, J., Moore, B.I., 2016d. Consistency between sun-induced chlorophyll fluorescence and gross primary production of vegetation in North America. Remote Sens. Environ. 183, 154–169.

Zhou, S., Zhang, Y., Caylor, K.K., Luo, Y., Xiao, X., Ciais, P., Huang, Y., Wang, G., 2016. Explaining inter-annual variability of gross primary productivity from plant phenology and physiology. Agric. For. Meteorol. 226–227, 246–256.